FLEXIBLE MULTIBODY ANALYSIS USING ABSOLUTE NODAL COORDINATE FORMULATION

A THESIS SUBMITTED TO
THE GRADUATE SCHOOL OF NATURAL AND APPLIED SCIENCES
OF
MIDDLE EAST TECHNICAL UNIVERSITY

BY

MUHAMMED ALİ ÇİFTÇİ

IN PARTIAL FULLFILLMENT OF THE REQUIREMENTS
FOR
THE DEGREE OF MASTER OF SCIENCE
IN
MECHANICAL ENGINEERING

SEPTEMBER 2014

Approval of the thesis:

FLEXIBLE MULTIBODY ANALYSIS USING ABSOLUTE NODAL COORDINATE FORMULATION

submitted by **MUHAMMED ALİ ÇİFTÇİ** in partial fulfillment of the requirements for the degree of **Master of Science in Mechanical Engineering Department, Middle East Technical University** by,

Prof. Dr. Canan Özgen _____
Dean, Graduate School of **Natural and Applied Sciences**

Prof. Dr. Süha Oral _____
Head of Department, **Mechanical Engineering**

Prof. Dr. Haluk Darendeliler _____
Supervisor, **Mechanical Engineering Dept., METU**

Prof. Dr. S. Kemal İder _____
Co-Supervisor, **Mechanical Engineering Dept., Çankaya University**

Examining Committee Members:

Prof. Dr. K. Levend Parnas _____
Mechanical Engineering Department, METU

Prof. Dr. Haluk Darendeliler _____
Mechanical Engineering Department, METU

Prof. Dr. S. Kemal İder _____
Mechanical Engineering Department, Çankaya University

Prof. Dr. Can Çoğun _____
Department of Mechatronics Engineering, Çankaya University

Asst. Prof. Dr. Hüsnü Dal _____
Mechanical Engineering Department, METU

Date: 03/09/2014

I hereby declare that all information in this document has been obtained and presented in accordance with academic rules and ethical conduct. I also declare that, as required by these rules and conduct, I have fully cited and referenced all material and results that are not original to this work.

Name, Last name : Muhammed Ali ÇİFTÇİ

Signature

ABSTRACT

FLEXIBLE MULTIBODY ANALYSIS USING ABSOLUTE NODAL COORDINATE FORMULATION

Çiftçi, Muhammed Ali
M.S., Department of Mechanical Engineering
Supervisor: Prof. Dr. Haluk Darendeliler
Co-supervisor: Prof. Dr. S. Kemal İder

September 2014, 95 Pages

The motion of the planar flexible multibody system with large deformation is analyzed by using the absolute nodal coordinate formulation (ANCF). For this purpose, flexible multibody systems consisting of beams are considered. In the conventional planar ANCF beam elements, there are two nodes located at the ends. Each element has eight degrees of freedom which consist of four global coordinates and four global slopes.

In this study, a planar beam element is developed with quadratic shape functions and new nodal configuration by using ANCF. In the developed element, an additional node is introduced to define the orientation and the shape of the beam so that neither angles nor slopes are used. At each element, six degrees of freedom exist. Since reduced degrees of freedom and quadratic shape functions are used, the element formulation is simplified considerably. Comparisons have been made between the developed beam element and the conventional ANCF beam element to see the

performances. Also, four-bar mechanism analyses have been made for small and large deformation cases by using ANCF beam element types and the floating frame of reference formulation.

Keywords: Flexible multi-body dynamics, the absolute nodal coordinate formulation, beam element, large deformation

ÖZ

MUTLAK NODAL KOORDİNAT FORMÜLASYONU KULLANILARAK ESNEK UZUVLU ÇOKLU CİSİM SİSTEMLERİN ANALİZİ

Çiftçi, Muhammed Ali
Yüksek Lisans, Makina Mühendisliği Bölümü
Tez Yöneticisi: Prof. Dr. Haluk Darendeliler
Ortak Tez Yöneticisi: Prof. Dr. S. Kemal İder

Eylül 2014, 95 Sayfa

Yüksek esnekliğe sahip çoklu cisimlerin hareket ve deformasyon analizlerinde mutlak nodal koordinat formülasyonu (MNKF) kullanılmaktadır. Bu amaçla düzlemsel kiriş elemanlarından oluşan çoklu cisim sistemler dikkate alınmıştır. Konvansiyonel MNKF kullanılan düzlemsel kiriş elemanlarının sonlarında iki adet düğüm noktası bulunmaktadır. Her bir eleman dört adet genel koordinat ve dört adet de eğim olmak üzere toplam sekiz adet serbestlik derecesine sahiptir.

Bu çalışmada ikinci dereceden şekil fonksiyonları ve yeni düğüm nokta düzeni kullanılarak düzlemsel bir MNKF kiriş elemanı tipi geliştirilmiştir. Yeni elemanda kiriş pozisyonunu ve şeklini tanımlamak için açı veya eğim kullanılmamış, ancak elemana yeni bir düğüm noktası eklenmiştir. Geliştirilen elemanda toplam altı adet serbestlik derecesi bulunmaktadır. Daha az sayıda serbestlik derecesi ve ikinci dereceden şekil fonksiyonlarının kullanılması sebebiyle eleman formülasyonu basitleşmiştir. Yeni eleman tipi ve konvansiyonel MNKF eleman tipinin

performanslarını karşılaştırmak için analizler yapılmıştır. Bunun yanında az esnek ve çok esnek dört çubuk mekanizmaları için çeşitli durumlarda analizler gerçekleştirilmiştir. Analizlerde MNKF eleman tipleri ve yüzen referans takımı formülasyonu kullanılmıştır.

Anahtar Kelimeler: Esnek çoklu cisim dinamiği, mutlak nodal koordinat formülasyonu, kiriş elemanı, yüksek deformasyon

To my family,

ACKNOWLEDGEMENTS

I would like to express my gratitude to my advisors Prof. Dr. Haluk Darendeliler and Prof. Dr. S. Kemal Ider for their support, guidance, patience and advices throughout the study.

Also, I would like to thank Halil Eryürek, Yetkin Telci and other colleagues at ASELSAN Inc. for their support and patience.

I am especially grateful to my colleague Dr. Emrah Gümüş who helped me in my thesis studies.

Finally, my deepest thanks go to my parents Aziz Çiftçi and Zehra Çiftçi, my brother Fatih Çiftçi and my sister Ayşe Nur Çiftçi for their endless love, encouragement and support in every time of my life.

TABLE OF CONTENTS

LIST OF TABLES

TABLES

LIST OF FIGURES

FIGURES

LIST OF ABBREVIATIONS

ANCF	: Absolute Nodal Coordinate Formulation
CAD	: Computer Aided Design
DAEs	: Differential Algebraic Equations
FFR	: Floating Frame of Reference Formulation
HHT	: Hilber-Hughes-Taylor Integration Method
ODEs	: Ordinary Differential Equations

CHAPTER 1

INTRODUCTION

1.1. Background and Motivation

Multibody systems are defined as the systems that have interconnected components. These components can be structural or force elements such as actuators, springs, dampers, etc. Mechanical systems like vehicles, machines, robotics, space structures and aircrafts are examples of multibody systems. These systems are very complex in most cases and consist of many sub-components that are kinematically constrained by joints. Large translations and rotational displacements may occur during the motion of such systems.

Multibody dynamics concerns with the dynamic models and calculations of the multibody systems. In the design phase of a system; effects of forces, interactions of bodies and dynamical behaviors of the components must be considered. Especially in today's world, design of complex systems should be cost effective, rapid and competitive so that analyses rather than costly tests and trials are preferable. Consequently, requirements of accurate and fast multibody system analyses lead researchers to this field, and weight of the analyses in the design phase are increasing compared to the past.

Multibody systems can be analyzed in two groups as rigid and flexible multibody systems. Rigid multibody systems consist of rigid bodies whereas flexible multibody systems consist of both rigid and deformable bodies. In rigid bodies, deformations are very small so that they have no effect to the system dynamical behaviors. The motion of rigid bodies is described by six generalized coordinates in the space. On

the other hand, deformations are not small to be ignored in the flexible bodies so that shapes, inertias and elastic properties change with time. In this case, non-linearities and number of coordinates needed in the mathematical model are very large compared to the rigid bodies, and computational effort becomes important [1-3].

Studies related to flexible multibody dynamics started in the early seventies with the need of simulating systems having flexible components [1]. New lightweight and elastic materials are frequently used nowadays. Also with high-speed demands, behaviors of systems may more likely to be flexible, and deformations should be concerned. In precise systems, like satellites and surgical robotic devices, even small deformations may affect the system overall behavior, and they must be considered. Although many flexible systems have small deformations under the force effects, large deformation problems become important in this era. Especially in the aerospace and railway applications, large deformation problems are needed to be investigated. For example, dynamic stability is very important in high-speed trains so that even interaction of a pantograph with flexible cables in a catenary system affects the system dynamical behavior [4]. Since deformations of cables in a catenary system can be relatively large, dynamic model should be constructed to handle large deformations in addition to large displacements.

Methods that are used in the analyses of flexible multibody systems can be given as the floating frame of reference formulation, the incremental finite element methods, the finite segment method, the large rotation vectors method and the absolute nodal coordinate formulation [1].

The finite element floating frame of reference formulation (FFR) is widely used in the computer programs that are used for the flexible multibody analyses. Well-known programs like Adams® and SimPack® can be given as examples that use this formulation in their background. The formulation is especially used for small deformation and large rotation problems [6]. In the formulation, two sets of coordinates are used. The first coordinate set describes the location and the orientation of the body in the global coordinate system whereas the other set is used

to describe the deformations with respect to the local body coordinate system. Finite element method is used to find the deformations of the body with respect to the local body coordinate system [1, 5].

In incremental finite element formulations, infinitesimal rotation angles are used to linearize the equations, and large rotations are represented by a sequence of small rotations so that linearization errors can be minimized. However, exact arbitrary rigid body motion cannot be obtained in this method due to the use of infinitesimal rotation angles [3]. This method is widely used in large deformation computational mechanics problems, and available in many commercial finite element softwares.

Finite segment method is used in flexible multibody system simulations especially in vehicle crash simulations. In the method, bodies are taken as rigid and segmented so that springs and dampers are used between these rigid segments to give the flexible features of the system. Using rigid bodies in the system simplifies the solution, but selection of the location and the size of these segments can be problematic. Also, spring and damper properties must be determined properly [1].

As mentioned before, linearization of the equations with infinitesimal rotations leads to some errors in the incremental methods. Large rotation vector formulation is proposed to avoid such errors. In the method, finite rotations of the element cross section are used as nodal coordinates instead of using infinitesimal rotations [1, 3]. Finite rotations are approximated with the interpolating polynomials. Nodal coordinates are used in the global coordinate system [3]. The method has some disadvantages. One of the problems is that rotations of the beam cross section are defined by the displacement coordinates in the case of beams so that using finite rotations of the cross section introduces redundancy. For this reason, singularity problems may arise while using this method. Also, shear values can be erroneous in the solutions [1]. Because of these problems, the method is not widely used in the flexible multibody simulations.

The absolute nodal coordinate formulation (ANCF) is introduced recently to solve large deformation and large rotation flexible multibody problems. In the method,

infinitesimal or finite rotations are not used. Instead, slopes are used to define the orientation of the element. Displacements and slopes are defined in the global coordinate system as nodal variables [3, 7]. Since global slopes are used in the formulation, linearization is not needed.

1.2. Research Objectives

Two types of elements are used in the finite element formulations as isoparametric and non-isoparametric elements. Body deformations and displacements can be described with the same order of approximation in the isoparametric elements whereas different orders of approximations are used in the non-isoparametric elements. Beam, plate and shell elements can be given as examples for non-isoparametric elements in the classical finite element formulations. With using infinitesimal rotation angles, nonlinear kinematic equations can be linearized in non-isoparametric elements, however this linearization leads to some errors. In such elements, large rotations cannot be handled efficiently [1, 3, 6]. Among the methods that are used in the flexible multibody analyses, the floating frame of reference formulation is the most popular one, since it can be applied widely and easily to the flexible multibody simulations without noticeable problems. In this method, small deformation problems can be handled, and exact rigid body motion can be obtained in the case of large rotations [1, 6]. But usage of the method is restricted to small deformation problems.

The absolute nodal coordinate formulation is used for both large deformation and large rotation problems. In the thesis, it is aimed to analyze planar flexible multibody systems to see the effects of small and large deformations on the system behaviors. Hence, the absolute nodal coordinate formulation is considered in this study to analyze the flexible multibody systems. The other objective is to develop a new computationally effective planar ANCF beam element type, and make comparisons.

1.3. Scope of the Thesis

In the thesis, a new computationally effective ANCF beam element is developed, and presented. Also, codes that can solve planar problems by ANCF beam elements are generated. Comparisons of the element types are made to see accuracies and performances. To see the effects of small and large deformations on the system behavior, and to compare the absolute nodal coordinate formulation and the floating frame of reference formulation, flexible four-bar mechanism analyses are used.

1.4. Thesis Outline

This thesis consists of eight chapters. Previous works and the theory are given in Chapter 2. In the theory, the Lagrangian equation, which is used in the dynamic equations of the multibody systems, is derived first. Then, the equations of motion are obtained by using the kinetic energy equation, the Lagrangian equation and the constraint equations. Also, generalized elastic and external force definitions are given in this chapter for the planar ANCF beam elements. Continuum mechanics approach with some simplifications is reviewed for the generalized elastic forces.

Mass matrices, stiffness matrices, generalized external force vectors and connectivity of the elements are described for the conventional and the new planar ANCF beam elements in Chapter 3 and Chapter 4 respectively.

In Chapter 5, numerical solution procedure used in the developed codes is explained. In the chapter, differential equations are stated first. Then, integration methods are mentioned with the details of Newmark's method. At the end, computational algorithm is given briefly.

In Chapter 6, performances of the new planar ANCF beam element and the conventional planar ANCF beam element are compared. In the analyses, the free falling pendulum and the four bar mechanism are used with large deformations.

In Chapter 7, four-bar mechanism analyses are made with the small-medium and large deformation cases. In these cases, the developed planar ANCF beam element

and the conventional planar ANCF beam element are compared. Also, the floating frame of reference formulation is compared with the absolute nodal coordinate formulation in the small-medium deformation cases.

At the end, summary, discussions and conclusion are given in Chapter 8. Recommendations for further research are also provided in this chapter.

CHAPTER 2

THE ABSOLUTE NODAL COORDINATE FORMULATION

2.1. Previous Works

In the absolute nodal coordinate formulation (ANCF), elements are iso-parametric so that both the body geometry and the deformations are approximated with the same shape function matrix. This feature differs from the classical finite element formulations that consider beam, plate and shell elements as non-isoparametric elements [7]. By using iso-parametric elements, exact rigid body motion can be obtained in the method [1].

In ANCF, centrifugal and Coriolis forces are zero unlike the floating frame of reference formulation. Also, the mass matrix is constant and symmetrical. However, elastic forces are highly-nonlinear and depend on the nodal coordinates [5]. To describe elastic forces, two main approaches are used in the literature. The first method is the local frame method whereas the other method is named as continuum mechanics approach.

If the planar beam element is considered, linear elastic model can be used in the local frame method. In this case, the Euler-Bernoulli beam theory can be used. Strain energy is found from the longitudinal and transverse deformations in the Euler-Bernoulli beam theory. Then, elastic forces can be found by taking the derivative of strain energy with respect to the vector of nodal coordinates. Longitudinal and transverse deformations are found from the geometry of the element in the local frame method. Since it is not easy to find deformations, two auxiliary local coordinate systems are proposed named as the pinned frame and the tangent frame [7, 9]. However, these local coordinate systems should not be confused with the local

coordinate systems that are used in the floating frame of reference formulation. Auxiliary local coordinate systems in ANCF are only used to find the expressions of the deformations, and does not affect the remaining solution. In the pinned frame, longitudinal and transverse deformations are found by using the coordinate system that is attached to the initial and last nodes of the element as shown in Figure 2.1.

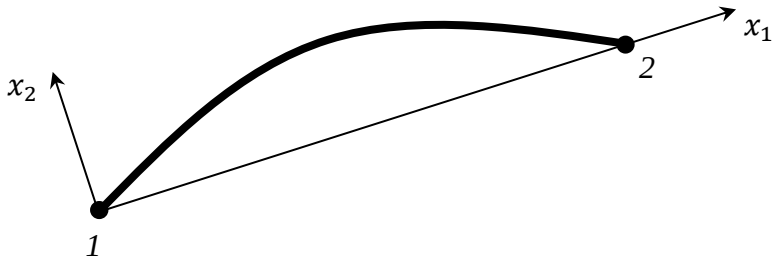

Figure 2.1 Coordinate system in the pinned frame.

In the tangent frame on the other hand, longitudinal and transverse deformations are found by the coordinate system that is attached to the first node, and tangent to the element as shown in Figure 2.2.

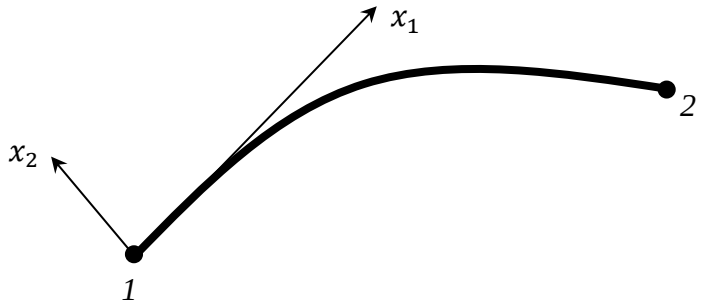

Figure 2.2 Coordinate system in the tangent frame.

In both frames, unit vectors that define x_1 and x_2 axes are found depends on the nodal variables, and used to find the deformations with the shape functions.

Berzeri et all. compare the pinned frame and the tangent frame approaches with the analyses results of the four bar mechanism [5]. In the analyses, same simulation is solved with different element numbers by the pinned frame and the tangent frame approaches. In the pinned frame approach, the results converge faster than the tangent frame approach as the element number is increased.

In the continuum mechanics approach, the strain energy is found by the strain-displacement relationships and the material properties. Then the elastic forces are obtained similarly by taking the partial derivative of the elastic energy with respect to the nodal coordinates. Unlike the other method, there is no need to use auxiliary coordinate system in the continuum mechanics approach [7].

Berzeri and Shabana developed simple models by using the continuum mechanics approach. These models are coupled by bending and axial deformations so that elastic forces are divided into longitudinal and transverse forces. They suggested three longitudinal and two transverse force models with different complexities. Since simpler force equations are used, analysis time can be decreased significantly. Also, more accurate results can be obtained since elastic non-linearity is considered in the strain-displacement relationship [7]. With some modifications of these simple models, analyses were made, and compared with the physical experiments by Wan-Suk Yoo et all [10]. In their experiments, a clamped thin cantilever beam with a point mass oscillates making small and large deformations. Results were recorded by a high-speed camera and a data acquisition system. Results of their experiments are in good agreement with the simulation results which shows the accuracy of the absolute nodal coordinate formulation.

In the planar ANCF beam element, shear deformations are neglected when the Euler-Bernoulli beam theory is used. In the Euler-Bernoulli beam theory, the cross section is assumed as rigid and perpendicular to the beam neutral axis. On the other hand, shear deformation is considered when Timoshenko beam theory is used. In the

Timoshenko beam theory, the cross section is not necessarily perpendicular to the beam neutral axis. But, the cross section is still rigid [11]. Shear deformable planar beam element that relaxes the assumptions in the Euler-Bernoulli and Timoshenko beam theories were developed in ANCF by Omar et al. [11]

In addition to the studies that have been made so far for the planar beam elements, researchers also focused on other element types like plate and shell elements in the absolute nodal coordinate formulation.

2.2. Theoretical Background

In the finite element formulations, geometry and dependent variables can be approximated with different orders. Depending on these different orders of approximations; elements are divided into three sub-categories as superparametric, isoparametric and subparametric elements [12]. In superparametric elements, the approximation of the body geometry has higher order than the approximation of the dependent variables. Contrast to superparametric elements, in subparametric elements the approximation of the body geometry has lower order than the dependent variables. In isoparametric elements, same approximation degree is used for both geometry and dependent variables.

In the classical finite element formulations, beams are not considered as isoparametric elements [5]. For example, in the Euler-Bernoulli beams, linear interpolation is used in the approximation of the geometry whereas cubic interpolation is used in the approximation of the transverse deflection [12]. Since the approximation of the geometry has lower order than the deflection, classical finite element formulation of the Euler-Bernoulli beams can be said as subparametric.

In such beam formulations, displacements and infinitesimal rotations are used as nodal coordinates that linearize the kinematic equations so that these elements cannot be used to model exact rigid body motion [1, 7, 13].

In the absolute nodal coordinate formulation (ANCF), displacements and deformations of the elements are defined in the global coordinate system by using the nodal coordinates and the shape functions [1]. Instead of using infinitesimal or finite rotations, slopes are used to define the orientation of the elements. With using the slopes, assumptions on the magnitude of element rotations are not necessary [7]. Since fixed coordinate system is used, coordinate transformation procedures are also not necessary [5, 7, 8].

2.2.1. Equations of Motion

From the Newton's second law, dynamic equilibrium of a particle k requires

$$\mathbf{F}^{(k)} = \dot{\mathbf{P}}^{(k)} \tag{2.1}$$

where $\mathbf{F}^{(k)}$ is the force acting on the particle k, and $\mathbf{P}^{(k)}$ is the momentum of the particle k. For the whole system which consists of n numbers of particles, the above equation can be written as

$$\sum_{k=1}^{n} \left(\mathbf{F}^{(k)} - \dot{\mathbf{P}}^{(k)}\right) \delta \mathbf{r}^{(k)} = \mathbf{0} \tag{2.2}$$

where $\delta \mathbf{r}^{(k)}$ is the virtual displacement of the particle k. Displacement of the particle k which is given below depends on a set of system generalized coordinates as

$$\mathbf{r}^{(k)} = \mathbf{r}^{(k)}\left(q_1^{(k)}, q_2^{(k)}, q_3^{(k)}, \ldots, q_m^{(k)}, t\right) \tag{2.3}$$

Then the virtual displacement of the particle k can be given as follows

$$\delta \mathbf{r}^{(k)} = \sum_{j=1}^{m} \frac{\partial \mathbf{r}^{(k)}}{\partial q_j^{(k)}} \delta q_j^{(k)} \tag{2.4}$$

If Equation (2.2) is written by using $\dot{\mathbf{P}}^{(k)} = m^{(k)}\ddot{\mathbf{r}}^{(k)}$ and Equation (2.4), it follows that

$$\sum_{k=1}^{n}\sum_{j=1}^{m}\left(\mathbf{F}^{(k)} - m^{(k)}\ddot{\mathbf{r}}^{(k)}\right)\frac{\partial \mathbf{r}^{(k)}}{\partial q_j^{(k)}}\delta q_j^{(k)} = 0 \tag{2.5}$$

where $m^{(k)}$ is the mass of the particle k. The generalized forces associated with the coordinates q_j are given as

$$Q_j = \sum_{k=1}^{n}\mathbf{F}^{(k)}\frac{\partial \mathbf{r}^{(k)}}{\partial q_j^{(k)}}\delta q_j \qquad j = 1, 2, \dots, m \tag{2.6}$$

Also, it can be shown that [3]:

$$\sum_{k=1}^{n}\left(m^{(k)}\ddot{\mathbf{r}}^{(k)}\frac{\partial \mathbf{r}^{(k)}}{\partial q_j^{(k)}}\right) = \sum_{k=1}^{n}\left[\frac{d}{dt}\left(m^{(k)}\dot{\mathbf{r}}^{(k)}\frac{\partial \mathbf{r}^{(k)}}{\partial q_j^{(k)}}\right) - m^{(k)}\dot{\mathbf{r}}^{(k)}\frac{\partial \dot{\mathbf{r}}^{(k)}}{\partial q_j^{(k)}}\right] \tag{2.7}$$

Differentiation of Equation (2.3) with respect to the time results

$$\dot{\mathbf{r}}^{(k)} = \frac{\partial \mathbf{r}^{(k)}}{\partial q_1^{(k)}}\dot{q}_1^{(k)} + \frac{\partial \mathbf{r}^{(k)}}{\partial q_2^{(k)}}\dot{q}_2^{(k)} + \frac{\partial \mathbf{r}^{(k)}}{\partial q_3^{(k)}}\dot{q}_3^{(k)} + \cdots + \frac{\partial \mathbf{r}^{(k)}}{\partial q_m^{(k)}}\dot{q}_m^{(k)} + \frac{\partial \mathbf{r}^{(k)}}{\partial t} \tag{2.8}$$

Then the partial derivative of Equation (2.8) with respect to $\dot{q}_j^{(k)}$ gives the following

$$\frac{\partial \dot{\mathbf{r}}^{(k)}}{\partial \dot{q}_j^{(k)}} = \frac{\partial \mathbf{r}^{(k)}}{\partial q_j^{(k)}} \tag{2.9}$$

Equation (2.7) can be arranged using Equation (2.9) as

$$\sum_{k=1}^{n}\left(m^{(k)}\ddot{\mathbf{r}}^{(k)}\frac{\partial \mathbf{r}^{(k)}}{\partial q_j^{(k)}}\right) = \sum_{k=1}^{n}\left\{\frac{d}{dt}\left[\frac{\partial}{\partial \dot{q}_j^{(k)}}\left(\frac{1}{2}m^{(k)}\dot{\mathbf{r}}^{(k)\mathrm{T}}\dot{\mathbf{r}}^{(k)}\right)\right] - \frac{\partial}{\partial q_j^{(k)}}\left(\frac{1}{2}m^{(k)}\dot{\mathbf{r}}^{(k)\mathrm{T}}\dot{\mathbf{r}}^{(k)}\right)\right\} \tag{2.10}$$

The kinetic energy of a particle k and the total kinetic energy of the system are defined as follows

$$T^{(k)} = \frac{1}{2}m^{(k)}\dot{\mathbf{r}}^{(k)\mathrm{T}}\dot{\mathbf{r}}^{(k)} \tag{2.11}$$

$$T = \sum_{k=1}^{n} T^{(k)} = \sum_{k=1}^{n}\frac{1}{2}m^{(k)}\dot{\mathbf{r}}^{(k)\mathrm{T}}\dot{\mathbf{r}}^{(k)} \tag{2.12}$$

Then, Equation (2.10) can be arranged using Equations (2.11) and (2.12) as

$$\sum_{k=1}^{n} m^{(k)}\ddot{\mathbf{r}}^{(k)}\frac{\partial \mathbf{r}^{(k)}}{\partial q_j^{(k)}} = \sum_{k=1}^{n}\left\{\frac{d}{dt}\left[\frac{\partial}{\partial \dot{q}_j^{(k)}}\left(T^{(k)}\right)\right] - \frac{\partial T^{(k)}}{\partial q_j^{(k)}}\right\} = \frac{d}{dt}\left(\frac{\partial T}{\partial \dot{q}_j}\right) - \frac{\partial T}{\partial q_j} \tag{2.13}$$

Substitution of Equations (2.6) and (2.13) into Equation (2.5) yields

$$\sum_{j=1}^{m}\left[\frac{d}{dt}\left(\frac{\partial T}{\partial \dot{q}_j}\right) - \frac{\partial T}{\partial q_j} - Q_j\right]\delta q_j = 0 \tag{2.14}$$

Also, Equation (2.14) can be described by matrix form as

$$\left[\frac{d}{dt}\left(\frac{\partial T}{\partial \dot{\mathbf{q}}}\right)-\frac{\partial T}{\partial \mathbf{q}}-\mathbf{Q}^{\mathrm{T}}\right]\delta\mathbf{q}=\mathbf{0} \tag{2.15}$$

Finally, Lagrange equation is achieved if the generalized coordinates of Equation (2.14) are independent, as below

$$\frac{d}{dt}\left(\frac{\partial T}{\partial \dot{\mathbf{q}}}\right)-\frac{\partial T}{\partial \dot{\mathbf{q}}}-\mathbf{Q}^{\mathrm{T}}=\mathbf{0} \tag{2.16}$$

In multibody systems, kinematic constraints exist, and virtual changes in the Equation (2.16) are not independent. In the dynamic equations, two methods are used to consider constraints. These are embedding technique and augmented formulation [3]. Augmented formulation is used in this study.

In the augmented formulation, Lagrange multipliers are used with the system generalized coordinates. The constraint equations can be given as

$$\boldsymbol{C}(\boldsymbol{q},t)=[C_1(\mathbf{q},t)\ C_2(\mathbf{q},t)\ C_3(\mathbf{q},t)\ \ldots\ C_n(\mathbf{q},t)]^{\mathrm{T}}=\ \mathbf{0} \tag{2.17}$$

For a virtual displacement $\delta\mathbf{q}$, Equation (2.17) leads to

$$\mathbf{C_q}\delta\mathbf{q}=\mathbf{0} \tag{2.18}$$

where $\mathbf{C_q}$ is the Jacobian matrix of the constraint equations. If Equation (2.18) is multiplied by a vector of Lagrange multipliers, $\boldsymbol{\lambda}$, it yields

$$\boldsymbol{\lambda}^{\mathrm{T}}\mathbf{C_q}\delta\mathbf{q}=[\lambda_1\ \ \lambda_2\ \ \lambda_3\ \ \ldots\ \lambda_n][C_1(\mathbf{q},t)\ C_2(\mathbf{q},t)\ \ldots\ C_n(\mathbf{q},t)]^{\mathrm{T}}\delta\mathbf{q}=\mathbf{0} \tag{2.19}$$

Equations (2.16) and (2.19) can be combined to give the following equation

$$\left[\frac{d}{dt}\left(\frac{\partial T}{\partial \dot{\mathbf{q}}}\right) - \frac{\partial T}{\partial \mathbf{q}} - \mathbf{Q}^{\mathrm{T}} + \boldsymbol{\lambda}^{\mathrm{T}}\mathbf{C}_{\mathbf{q}}\right]\delta\mathbf{q} = \mathbf{0} \tag{2.20}$$

or it can be given as

$$\frac{d}{dt}\left(\frac{\partial T}{\partial \dot{\mathbf{q}}}\right) - \frac{\partial T}{\partial \mathbf{q}} - \mathbf{Q}^{\mathrm{T}} + \boldsymbol{\lambda}^{\mathrm{T}}\mathbf{C}_{\mathbf{q}} = \mathbf{0} \tag{2.21}$$

The undeformed and deformed configurations of the ANCF beam element is given in Figure 2.3. In the absolute nodal coordinate formulation, global position vector $\mathbf{r}^{(ki)}$ of an arbitrary point K on the i^{th} beam element in the body k is defined by the global shape function matrix, $\mathbf{S}^{(ki)}$, and the vector of nodal coordinates of the element, $\mathbf{e}^{(ki)}$, as

$$\mathbf{r}^{(ki)} = \begin{bmatrix} r_{\mathrm{X}_1}^{(ki)} \\ r_{\mathrm{X}_2}^{(ki)} \end{bmatrix} = \mathbf{S}^{(ki)}\mathbf{e}^{(ki)} \tag{2.22}$$

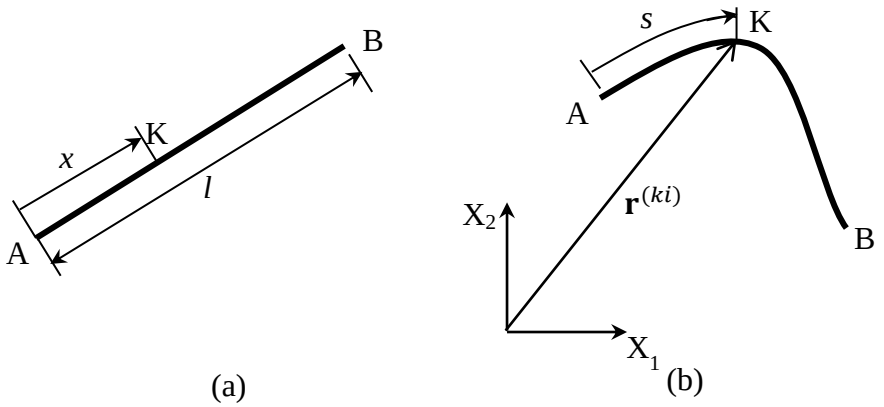

Figure 2.3 Undeformed (a) and deformed (b) configurations of the ANCF beam element.

The kinetic energy of the element are given in the undeformed state as [3, 5, 7-9]

$$T^{(ki)} = \frac{1}{2}\int_{V_0} \rho_0 \dot{\mathbf{r}}^{(ki)\mathrm{T}} \dot{\mathbf{r}}^{(ki)} \mathrm{d}V_0 = \frac{1}{2}\int_{V_0} \rho_0 \left(\mathbf{S}^{(ki)\mathrm{T}} \dot{\mathbf{e}}^{(ki)\mathrm{T}}\right)\left(\mathbf{S}^{(ki)} \dot{\mathbf{e}}^{(ki)}\right)\mathrm{d}V_0$$
$$= \frac{1}{2}\dot{\mathbf{e}}^{(ki)\mathrm{T}}\left(\int_{V_0} \rho_0 \mathbf{S}^{(ki)\mathrm{T}} \mathbf{S}^{(ki)}\, \mathrm{d}V_0\right)\dot{\mathbf{e}}^{(ki)} \tag{2.23}$$
$$= \frac{1}{2}\,\dot{\mathbf{e}}^{(ki)\mathrm{T}} \mathbf{M}^{(ki)}\,\dot{\mathbf{e}}^{(ki)}$$

where ρ_0 is the density, V_0 is the volume in the undeformed state, and $\mathbf{M}^{(ki)}$ is the mass matrix of the element. Knowing the fact that $\int_{V_0} \rho_0 \mathrm{d}V_0 = \int_V \rho\, \mathrm{d}V$, and using the Equation (2.23), the constant mass matrix of the element at any time can be obtained as follows

$$\mathbf{M}^{(ki)} = \int_V \rho \mathbf{S}^{(ki)\mathrm{T}} \mathbf{S}^{(ki)}\, \mathrm{d}V \tag{2.24}$$

Equation (2.24) can also be expressed as

$$\mathbf{M}^{(ki)} = \int_V \rho \mathbf{S}^{(ki)\mathrm{T}} \mathbf{S}^{(ki)}\, \mathrm{d}V = m\int_0^1 \mathbf{S}^{(ki)\mathrm{T}} \mathbf{S}^{(ki)}\, \mathrm{d}\xi \tag{2.25}$$

Here m is defined as the total mass of the beam element, $\xi = x/l$, x is the coordinate of an arbitrary point on the element and l is the length of the beam in the undeformed configuration.

For ANCF beam elements, Equation (2.16) can be arranged by using Equation (2.23) as follows

$$\frac{d}{dt}\left[\frac{\partial}{\partial \dot{\mathbf{e}}^{(ki)}}\left(\frac{1}{2}\,\dot{\mathbf{e}}^{(ki)\mathrm{T}} \mathbf{M}^{(ki)}\,\dot{\mathbf{e}}^{(ki)}\right)\right]^{\mathrm{T}} - \left[\frac{\partial}{\partial \mathbf{e}^{(ki)}}\left(\frac{1}{2}\,\dot{\mathbf{e}}^{(ki)\mathrm{T}} \mathbf{M}^{(ki)}\,\dot{\mathbf{e}}^{(ki)}\right)\right]^{\mathrm{T}} = \mathbf{Q}^{(ki)} \tag{2.26}$$

Equation (2.26) can be rearranged as

$$\mathbf{M}^{(ki)}\ddot{\mathbf{e}}^{(ki)} + \dot{\mathbf{M}}^{(ki)}\dot{\mathbf{e}}^{(ki)} - \left[\frac{\partial}{\partial \mathbf{e}^{(ki)}}\left(\frac{1}{2}\,\dot{\mathbf{e}}^{(ki)\mathrm{T}}\mathbf{M}^{(ki)}\,\dot{\mathbf{e}}^{(ki)}\right)\right]^{\mathrm{T}} = \mathbf{Q}^{(ki)} \tag{2.27}$$

where centrifugal and Coriolis inertia forces, named as $\mathbf{Q_v}^{(ki)}$, are represented as

$$\mathbf{Q_v}^{(ki)} = \dot{\mathbf{M}}^{(ki)}\dot{\mathbf{e}}^{(ki)} - \left[\frac{\partial}{\partial \mathbf{e}^{(ki)}}\left(\frac{1}{2}\,\dot{\mathbf{e}}^{(ki)\mathrm{T}}\mathbf{M}^{(ki)}\,\dot{\mathbf{e}}^{(ki)}\right)\right]^{\mathrm{T}} \tag{2.28}$$

Since the mass matrix is constant in the absolute nodal coordinate formulation, centrifugal and Coriolis inertia force matrix given in Equation (2.28) is zero. Then Lagrange equation of the i^{th} ANCF beam element in the body k is simplified as follows

$$\mathbf{M}^{(ki)}\ddot{\mathbf{e}}^{(ki)} = \mathbf{Q}^{(ki)} \tag{2.29}$$

If the elements of bodies in the system are formulated by the absolute nodal coordinate formulation, then Equation (2.21) is simplified as

$$\mathbf{M}\ddot{\mathbf{q}} + \mathbf{C_q}^{\mathrm{T}}\boldsymbol{\lambda} = \mathbf{Q} \tag{2.30}$$

Taking second time derivative of the constraint equations yields

$$\mathbf{C}_q\ddot{\mathbf{q}} = \mathbf{H} \tag{2.31}$$

where **H** in Equation (2.31) is the vector resulting from the second time derivative of the constraint equations. Since constraints are time independent in most cases, it becomes zero vector. Equations of motion for the system composed of Equation (2.30) and (2.31) can be combined as follows

$$\begin{bmatrix} \mathbf{M} & \mathbf{C}_q{}^T \\ \mathbf{C}_q & \mathbf{0} \end{bmatrix} \begin{bmatrix} \ddot{\mathbf{q}} \\ \boldsymbol{\lambda} \end{bmatrix} = \begin{bmatrix} \mathbf{Q} \\ \mathbf{H} \end{bmatrix} \tag{2.32}$$

2.2.2. Generalized Elastic Forces for the planar ANCF Beam Element

Deformations can be defined in the absolute nodal coordinate formulation by two approaches. In the first approach, a local element coordinate system is used to define deformations and elastic forces. Pinned frame and tangent frame can be used as local element coordinate systems. In the pinned frame, one axis passes through the first and last nodes whereas other axis is perpendicular to the first axis. In the tangent frame, one axis is selected to be tangent to the beam at the first node, and other is perpendicular to the first one. The first approach with the local coordinates gives a more complex procedure and equations for the elastic forces [5, 11]. The second approach, named as continuum mechanics approach, does not require a local coordinate system. In this approach elastic non-linearity is also considered in the strain-displacement relationship so that more accurate results can be obtained [7]. In this study, the continuum mechanics approach with the classical Euler-Bernoulli beam theory is used for the generalized elastic force equations.

The total strain energy of the beam element can be written as follows

$$U_s^{(ki)} = U_{sl}^{(ki)} + U_{st}^{(ki)} \tag{2.33}$$

where the strain energy due to the stretch for the points on the mid-surface, $U_{sl}^{(ki)}$, and the strain energy due to the transverse deformation, $U_{st}^{(ki)}$, are [7, 14]

$$U_{sl}^{(ki)} = \frac{1}{2}\int_0^l EA{\varepsilon_l}^2 \mathrm{d}x \tag{2.34}$$

$$U_{st}^{(ki)} = \frac{1}{2}\int_0^l EI\kappa^2 \mathrm{d}x \tag{2.35}$$

Here E is the Young's modulus for isotropic materials, A is the cross sectional area of the beam element ε_l is the strain due to the stretch for the points on the mid-surface, I is the second moment of area, and κ is the curvature of the beam.

Then the generalized elastic force vector due to the longitudinal deformations, $\mathbf{Q}_{sl}^{(ki)}$, and the transverse deformations, $\mathbf{Q}_{st}^{(ki)}$, can be determined by using the partial derivatives of the corresponding strain energies with respect to the vector of nodal coordinates as

$$\mathbf{Q}_{s}^{(ki)} = \mathbf{Q}_{sl}^{(ki)} + \mathbf{Q}_{st}^{(ki)} \tag{2.36}$$

where

$$\mathbf{Q}_{sl}^{(ki)} = -\left(\frac{\partial U_{sl}^{(ki)}}{\partial \mathbf{e}^{(ki)}}\right)^{\mathrm{T}} = -\mathbf{K}_{sl}^{(ki)}\mathbf{e}^{(ki)} \tag{2.37}$$

$$\mathbf{Q}_{st}^{(ki)} = -\left(\frac{\partial U_{st}^{(ki)}}{\partial \mathbf{e}^{(ki)}}\right)^{\mathrm{T}} = -\mathbf{K}_{st}^{(ki)}\mathbf{e}^{(ki)} \tag{2.38}$$

In the above equations $\mathbf{K}_{sl}^{(ki)}$ and $\mathbf{K}_{st}^{(ki)}$ are defined as the longitudinal and transverse stiffness matrices.

Infinitesimal arc length of the deformed beam element can be found by [7]

$$\mathrm{d}s = \sqrt{\mathbf{r}'^{(ki)^{\mathrm{T}}}\mathbf{r}'^{(ki)}}\mathrm{d}x \tag{2.39}$$

where s is the arc length, and $\mathbf{r}'^{(ki)}$ is given below

$$\mathbf{r}'^{(ki)} = \frac{\mathrm{d}\mathbf{r}^{(ki)}}{\mathrm{d}x} \tag{2.40}$$

The Lagrangian strain for a planar beam is defined as follows

$$\mathrm{d}s^2 - \mathrm{d}x^2 = 2\mathrm{d}x\varepsilon_l\mathrm{d}x \tag{2.41}$$

From Equations (2.39) and (2.41), the strain due to stretch can be determined by

$$\varepsilon_l = \frac{1}{2}\left(\mathbf{r}'^{(ki)\mathrm{T}}\mathbf{r}'^{(ki)} - 1\right) = \frac{1}{2}\left(\mathbf{e}^{(ki)\mathrm{T}}\mathbf{S}'^{(ki)\mathrm{T}}\mathbf{S}'^{(ki)}\mathbf{e}^{(ki)} - 1\right) \tag{2.42}$$

where $\mathbf{S}'$ is the derivative of the shape function with respect to *x*. If $\mathbf{e}_r$ represents the nodal coordinate vector corresponding to an arbitrary rigid body position, it can be shown that

$$\mathbf{e}_r{}^{\mathrm{T}}\mathbf{S}'^{(ki)\mathrm{T}}\mathbf{S}'^{(ki)}\mathbf{e}_r = 1 \tag{2.43}$$

Also, it can be said that $\mathbf{e}^{(ki)\mathrm{T}}\mathbf{S}'^{(ki)\mathrm{T}}\mathbf{S}'^{(ki)}\mathbf{e}^{(ki)}$ is very close to one, and Equation (2.42) is difficult to determine accurately [7]. Then Equation (2.42) can be rearranged using Equation (2.43) as

$$\begin{aligned}\varepsilon_l &= \frac{1}{2}\left(\mathbf{e}^{(ki)\mathrm{T}}\mathbf{S}'^{(ki)\mathrm{T}}\mathbf{S}'^{(ki)}\mathbf{e}^{(ki)} - 1\right)\\ &= \frac{1}{2}\left(\mathbf{e}^{(ki)\mathrm{T}}\mathbf{S}'^{(ki)\mathrm{T}}\mathbf{S}'^{(ki)}\mathbf{e}^{(ki)} - \mathbf{e}_r{}^{\mathrm{T}}\mathbf{S}'^{(ki)\mathrm{T}}\mathbf{S}'^{(ki)}\mathbf{e}_r\right)\\ &= \frac{1}{2}\left(\mathbf{e}^{(ki)} - \mathbf{e}_r\right)^{\mathrm{T}}\mathbf{S}'^{(ki)\mathrm{T}}\mathbf{S}'^{(ki)}\left(\mathbf{e}^{(ki)} + \mathbf{e}_r\right)\end{aligned} \tag{2.44}$$

From Equation (2.42) it can be found that

$$\left(\frac{\partial\varepsilon_l}{\partial\mathbf{e}^{(ki)}}\right)^{\mathrm{T}} = \mathbf{S}'^{(ki)\mathrm{T}}\mathbf{S}'^{(ki)}\mathbf{e}^{(ki)} \tag{2.45}$$

Using Equations (2.34), (2.37) and (2.45), the vector of generalized elastic forces due to the stretching is determined as follows

$$\mathbf{Q}_{sl}^{(ki)} = \int_0^l EA\varepsilon_l \, \mathbf{S}'^{(ki)^{\mathrm{T}}} \mathbf{S}'^{(ki)} \mathbf{e}^{(ki)} \mathrm{d}x \tag{2.46}$$

Also, the longitudinal stiffness matrix is found by Equations (2.37) and (2.46) as

$$\mathbf{K}_{sl}^{(ki)} = \int_0^l EA\varepsilon_l \mathbf{S}'^{(ki)^{\mathrm{T}}} \mathbf{S}'^{(ki)} \mathrm{d}x \tag{2.47}$$

Serret-Frenet formulas [15, 16] can be used to take bending effect into consideration. The curvature of the beam is described by

$$\kappa = \left| \frac{\mathrm{d}^2 \mathbf{r}^{(ki)}}{\mathrm{d}s^2} \right| \tag{2.48}$$

In the case of small longitudinal deformations, the curvature given in Equation (2.48) can be simplified as follows [7]

$$\kappa = \left| \frac{\mathrm{d}^2 \mathbf{r}^{(ki)}}{\mathrm{d}s^2} \right| \cong \left| \frac{\mathrm{d}^2 \mathbf{r}^{(ki)}}{\mathrm{d}x^2} \right| = \left| \mathbf{r}''^{(ki)} \right| \tag{2.49}$$

Then the equation given below is found by using Equation (2.49) as

$$\kappa^2 = \mathbf{e}^{(ki)^{\mathrm{T}}} \mathbf{S}''^{(ki)^{\mathrm{T}}} \mathbf{S}''^{(ki)} \mathbf{e}^{(ki)} \tag{2.50}$$

where $\mathbf{S}''^{(ki)} = d^2\mathbf{S}^{(ki)} \, / \, dx^2$. Using Equations (2.35), (2.38) and (2.50), the vector of generalized elastic forces due to the transverse deformations is determined as follows

$$\mathbf{Q}_{st}^{(ki)} = \int_0^l EI\, \mathbf{S}''^{(ki)^{\mathrm{T}}} \mathbf{S}''^{(ki)} \mathbf{e}^{(ki)} \mathrm{d}x \tag{2.51}$$

Also, the transverse stiffness matrix is found by using Equations (2.38) and (2.51) as

$$\mathbf{K}_{st}^{(ki)} = \int_0^l EI \mathbf{S}''^{(ki)^{\mathrm{T}}} \mathbf{S}''^{(ki)} \mathrm{d}x \tag{2.52}$$

In the case of large longitudinal deformation, Equation (2.49) is no longer valid. In this case, the following equation can be used for the curvature as [7]

$$\kappa = \frac{\mathbf{e}^{(ki)^{\mathrm{T}}} \mathbf{S}_{\boldsymbol{t}}^{(ki)} \mathbf{e}^{(ki)}}{f^3} \tag{2.53}$$

where

$$\mathbf{S}_{\boldsymbol{t}}^{(ki)} = \frac{1}{2}\left[\left(\mathbf{S}'^{(ki)^{\mathrm{T}}} \tilde{\mathbf{I}} \mathbf{S}'^{(ki)}\right) + \left(\mathbf{S}'^{(ki)^{\mathrm{T}}} \tilde{\mathbf{I}} \mathbf{S}''^{(ki)}\right)^{\mathrm{T}}\right] \tag{2.54}$$

and f is the deformation gradient that is given below

$$f = \frac{\mathrm{d}s}{\mathrm{d}x} \tag{2.55}$$

In the Equation (2.54), $\tilde{\mathbf{I}}$ is defined as

$$\tilde{\mathbf{I}} = \begin{bmatrix} 0 & -1 \\ 1 & 0 \end{bmatrix} \tag{2.56}$$

In the case of large longitudinal deformation, Equation (2.54) can be used to find the strain energy and stiffness matrix. Since Equation (2.54) leads to a complex expression for the elastic forces, it can be simplified further by assuming the deformation gradient is constant [7].

2.2.3. Generalized External Forces for the planar ANCF Beam Element

Virtual work due to externally applied force acting on an arbitrary point on the element is given as follows

$$\mathbf{F}^{\mathrm{T}}\delta\mathbf{r}^{(ki)} = \mathbf{F}^{\mathbf{T}}\mathbf{S}^{(ki)}\boldsymbol{\delta}\mathbf{e}^{(ki)} = \mathbf{Q}_{\boldsymbol{e}}{}^{\mathbf{T}}\boldsymbol{\delta}\mathbf{e}^{(ki)} \tag{2.57}$$

From the above equation, generalized external force vector is defined as

$$\mathbf{Q}_e = \mathbf{S}^{(ki)^{\mathrm{T}}}\mathbf{F} \tag{2.58}$$

CHAPTER 3

THE CONVENTIONAL PLANAR ANCF BEAM ELEMENT

3.1. The Nodal Coordinates and the Shape Function Matrix for the Conventional Planar ANCF Beam Element

The conventional beam element i of the body k in undeformed and deformed configurations is given in Figure 3.1. The global position vector, $\mathbf{r}^{(ki)}$, of an arbitrary point K on the element is found by using the global shape function, $\mathbf{S}^{(ki)}$, and the vector of nodal coordinates, $\mathbf{e}^{(ki)}$, as given in the Equation (2.22).

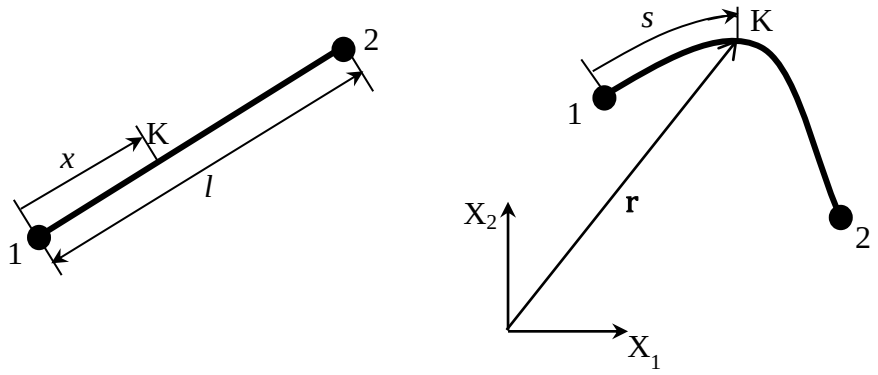

Figure 3.1 Undeformed (a) and deformed (b) configurations of the conventional planar ANCF beam element.

Here the vector of nodal coordinates for the conventional planar beam element is given as [5, 7-9, 13]

$$\mathbf{e}^{(ki)} = \begin{bmatrix} e_1^{(ki)} & e_2^{(ki)} & e_3^{(ki)} & e_4^{(ki)} & e_5^{(ki)} & e_6^{(ki)} & e_7^{(ki)} & e_8^{(ki)} \end{bmatrix}^{\mathrm{T}} \tag{3.1}$$

where global displacements and slopes are

$$\begin{gathered} e_1^{(ki)} = {}^1r_{\mathrm{X}_1}^{(ki)}, \quad e_2^{(ki)} = {}^1r_{\mathrm{X}_2}^{(ki)}, \quad e_3^{(ki)} = \frac{\partial {}^1r_{\mathrm{X}_1}^{(ki)}}{\partial x}, \quad e_4^{(ki)} = \frac{\partial {}^1r_{X}^{(ki)}}{\partial x} \\ e_5^{(ki)} = {}^2r_{\mathrm{X}_1}^{(ki)}, \quad e_6^{(ki)} = {}^2r_{\mathrm{X}_2}^{(ki)}, \quad e_7^{(ki)} = \frac{\partial {}^2r_{\mathrm{X}_1}^{(ki)}}{\partial x}, \quad e_8^{(ki)} = \frac{\partial {}^2r_{\mathrm{X}_2}^{(ki)}}{\partial x} \end{gathered} \tag{3.2}$$

Left superscripts in the above equations represent the node numbers in the element. To approximate the geometry and deformation, cubic polynomials are used in the global shape function matrix. It can be given as below [5, 7-9, 13]

$$\mathbf{S}^{(ki)} = \begin{bmatrix} s_1 & 0 & s_2 & 0 & s_3 & 0 & s_4 & 0 \\ 0 & s_1 & 0 & s_2 & 0 & s_3 & 0 & s_4 \end{bmatrix} \tag{3.3}$$

where,

$$\begin{gathered} s_1 = 1 - 3\xi^2 + 2\xi^3, \quad s_2 = l(\xi - 2\xi^2 + \xi^3) \\ s_3 = 3\xi^2 - 2\xi^3, \quad s_4 = l(\xi^3 - \xi^2) \end{gathered} \tag{3.4}$$

Global shape function matrix that is used in the ANCF contains all rigid body modes so that arbitrary rigid body translations and rotations are fully described.

3.2. Mass Matrix of the Conventional Planar ANCF Beam Element

The mass matrix can be found explicitly by arranging the Equation (2.25) with the vector of nodal coordinates and the shape function matrix for the conventional planar ANCF beam element as [13]

$$\mathbf{M}^{(ki)} = m \begin{bmatrix} \frac{13}{35} & 0 & \frac{11l}{210} & 0 & \frac{9}{70} & 0 & \frac{-13l}{420} & 0 \\ 0 & \frac{13}{35} & 0 & \frac{11l}{210} & 0 & \frac{9}{70} & 0 & \frac{-13l}{420} \\ \frac{11l}{210} & 0 & \frac{l^2}{105} & 0 & \frac{13l}{420} & 0 & \frac{-l^2}{140} & 0 \\ 0 & \frac{11l}{210} & 0 & \frac{l^2}{105} & 0 & \frac{13l}{420} & 0 & \frac{-l^2}{140} \\ \frac{9}{70} & 0 & \frac{13l}{420} & 0 & \frac{13}{56} & 0 & \frac{-11l}{210} & 0 \\ 0 & \frac{9}{70} & 0 & \frac{13l}{420} & 0 & \frac{13}{35} & 0 & \frac{-11l}{210} \\ \frac{-13l}{420} & 0 & \frac{-l^2}{140} & 0 & \frac{-11l}{210} & 0 & \frac{l^2}{105} & 0 \\ 0 & \frac{-13l}{420} & 0 & \frac{-l^2}{140} & 0 & \frac{-11l}{210} & 0 & \frac{l^2}{105} \end{bmatrix} \tag{3.5}$$

3.3. Stifness Matrices of the Conventional Planar ANCF Beam Element

If E and A are constant, Equation (2.47) can be arranged as follows

$$\mathbf{K}_{sl}^{(ki)} = EA \int_0^l \varepsilon_l \mathbf{S}'^{(ki)\mathrm{T}} \mathbf{S}'^{(ki)} \mathrm{d}x = EAl \int_0^1 \varepsilon_l \mathbf{S}'^{(ki)\mathrm{T}} \mathbf{S}'^{(ki)} \mathrm{d}\xi \tag{3.6}$$

If Equation (2.44) is used with an arbitrary rigid body displacement vector, which can be given as $\mathbf{e}_r = [0\ 0\ 1\ 0\ l\ 0\ 1\ 0]^{\mathrm{T}}$, the longitudinal stiffness matrix can be written explicitly as [7]

$$\mathbf{K}_{sl}^{(ki)} = \frac{EA}{l}\begin{bmatrix} K_{sl}^{A} & 0 & K_{sl}^{B} & 0 & -K_{sl}^{A} & 0 & K_{sl}^{C} & 0 \\ & K_{sl}^{A} & 0 & K_{sl}^{B} & 0 & -K_{sl}^{A} & 0 & K_{sl}^{C} \\ & & K_{sl}^{D} & 0 & -K_{sl}^{B} & 0 & K_{sl}^{E} & 0 \\ & & & K_{sl}^{D} & 0 & -K_{sl}^{B} & 0 & K_{sl}^{E} \\ & & sym & & K_{sl}^{A} & 0 & -K_{sl}^{C} & 0 \\ & & & & & K_{sl}^{A} & 0 & -K_{sl}^{C} \\ & & & & & & K_{sl}^{F} & 0 \\ & & & & & & & K_{sl}^{F} \end{bmatrix} \tag{3.7}$$

where

$$K_{sl}^{A} = \frac{3}{70l^2}\left(a^2 + b^2 - 14l^2 - 6a_x c_x - 6b_x c_x - 6a_y c_y - 6b_y c_y + 24c^2\right) \tag{3.8}$$

$$K_{sl}^{B} = \frac{1}{280l}\left(b^2 - a^2 + 2a_x b_x + 2a_y b_y - 14l^2 - 24a_x c_x - 24a_y c_y + 36c^2\right) \tag{3.9}$$

$$K_{sl}^{C} = \frac{1}{280l}\left(a^2 - b^2 + 2a_x b_x + 2a_y b_y - 14l^2 - 24b_x c_x - 24b_y c_y + 36c^2\right) \tag{3.10}$$

$$K_{sl}^{D} = \frac{1}{420}\left(12a^2 + b^2 - 3a_x b_x - 3a_y b_y - 28l^2 + 3a_x c_x - 3b_x c_x + 3a_y c_y - 3b_y c_y + 18c^2\right) \tag{3.11}$$

$$K_{sl}^{E} = -\frac{1}{840}\left(3a^2 + 3b^2 - 4a_x b_x - 4a_y b_y - 14l^2 + 6a_x c_x + 6b_x c_x + 6a_y c_y + 6b_y c_y\right) \tag{3.12}$$

$$K_{sl}^{F} = \frac{1}{420}\left(a^2 + 12b^2 - 3a_x b_x - 3a_y b_y - 28l^2 - 3a_x c_x + 3b_x c_x - 3a_y c_y + 3b_y c_y + 18c^2\right) \tag{3.13}$$

and

$$a_x = le_3^{(ki)}, \qquad a_y = le_4^{(ki)}, \qquad a = \sqrt{{a_x}^2 + {a_y}^2} \tag{3.14}$$

$$b_x = le_7^{(ki)}, \qquad b_y = le_8^{(ki)}, \qquad b = \sqrt{{b_x}^2 + {b_y}^2} \tag{3.15}$$

$$c_x = e_5^{(ki)} - e_1^{(ki)}, \qquad c_y = e_6^{(ki)} - e_2^{(ki)}, \qquad c = \sqrt{{c_x}^2 + {c_y}^2} \tag{3.16}$$

Assuming E and I are constant, Equation (2.52) can be arranged as below

$$\mathbf{K}_{st}^{(ki)} = EI\int_0^l \mathbf{S}''^{(ki)\mathrm{T}}\mathbf{S}''^{(ki)}\mathrm{d}x = \frac{1}{2}EIl\int_0^1 \mathbf{S}''^{\mathrm{T}}\mathbf{S}''\mathrm{d}\xi \tag{3.17}$$

Then the transverse stiffness matrix is given in matrix form explicitly as

$$\mathbf{K}_{st}^{(ki)} = \frac{EI}{l^3}\begin{bmatrix} 12 & 0 & 6l & 0 & -12 & 0 & 6l & 0 \\ & 12 & 0 & 6l & 0 & -12 & 0 & 6l \\ & & 4l^2 & 0 & -6l & 0 & 2l^2 & 0 \\ & & & 4l^2 & 0 & -6l & 0 & 2l^2 \\ & & & & 12 & 0 & -6l & 0 \\ & & sym & & & 12 & 0 & -6l \\ & & & & & & 4l^2 & 0 \\ & & & & & & & 4l^2 \end{bmatrix} \tag{3.18}$$

3.4. Generalized External Forces for the Conventional Planar ANCF Beam Element

Equation (2.58) is used to get generalized external force vector for the conventional ANCF beam element.

For the gravitational force $\mathbf{F}_{\mathrm{g}} = mg\mathbf{u}$,where $\mathbf{u}$ is the unit vector along the gravitational direction with respect to the global coordinate system, and g is the gravitational acceleration, the generalized external force due to the gravitation is found explicitly by using Equation (2.58) as follows

$$\mathbf{Q}_e^{(ki)} = mg \begin{bmatrix} \frac{1}{2} & 0 & \frac{l}{12} & 0 & \frac{1}{2} & 0 & -\frac{l}{12} & 0 \\ 0 & \frac{1}{2} & 0 & \frac{l}{2} & 0 & \frac{1}{2} & 0 & -\frac{l}{12} \end{bmatrix}^{\mathrm{T}} \mathbf{u} \tag{3.19}$$

Assuming a moment M acts on a cross-section of the beam, virtual work due to the moment can be given as

$$M\delta\alpha \tag{3.20}$$

Here $\delta\alpha$ is a virtual angle change as a result of bending moment. Transformation matrix, **T**, is defined for the orientation of a coordinate system attached to the cross-section of the beam as

$$\mathbf{T} = \begin{bmatrix} \cos\alpha & -\sin\alpha \\ \sin\alpha & \cos\alpha \end{bmatrix} = \frac{1}{\sqrt{d}} \begin{bmatrix} \frac{\partial r_{\mathrm{X}_1}^{(ki)}}{\partial x} & -\frac{\partial r_{\mathrm{X}_2}^{(ki)}}{\partial x} \\ \frac{\partial r_{\mathrm{X}_2}^{(ki)}}{\partial x} & \frac{\partial r_{\mathrm{X}_1}^{(ki)}}{\partial x} \end{bmatrix} \tag{3.21}$$

where

$$d = \left(\frac{\partial r_{\mathrm{X}_1}^{(ki)}}{\partial x}\right)^2 + \left(\frac{\partial r_{\mathrm{X}_2}^{(ki)}}{\partial x}\right)^2 \tag{3.22}$$

Equation (3.21) yields

$$\cos\alpha = \frac{1}{\sqrt{d}}\frac{\partial r_{X_1}^{(ki)}}{\partial x} \quad , \qquad \sin\alpha = \frac{1}{\sqrt{d}}\frac{\partial r_{X_2}^{(ki)}}{\partial x} \tag{3.23}$$

From Equation (3.23), it can be shown that

$$\delta(\cos\alpha) = -\sin\alpha\,\delta\alpha = \delta\left(\frac{1}{\sqrt{d}}\right)\frac{\partial r_{X_1}^{(ki)}}{\partial x} + \frac{1}{\sqrt{d}}\,\delta\left(\frac{\partial r_{X_1}^{(ki)}}{\partial x}\right) \tag{3.24}$$

From Equations (3.22), (3.23) and (3.24); virtual change in the orientation angle is found as

$$\delta\alpha = \frac{\frac{\partial r_{X_1}^{(ki)}}{\partial x}\delta\left(\frac{\partial r_{X_2}^{(ki)}}{\partial x}\right) - \frac{\partial r_{X_2}^{(ki)}}{\partial x}\delta\left(\frac{\partial r_{X_1}^{(ki)}}{\partial x}\right)}{d} \tag{3.25}$$

If a moment is applied at first node of the element, Equation (3.25) can be determined as follows

$$\begin{aligned}\delta\alpha &= \frac{e_3^{(ki)}\delta\left(e_4^{(ki)}\right) - e_4^{(ki)}\delta\left(e_3^{(ki)}\right)}{{e_3^{(ki)}}^2 + {e_4^{(ki)}}^2} \\ &= \begin{bmatrix} 0 & 0 & \dfrac{-e_4^{(ki)}}{{e_3^{(ki)}}^2 + {e_4^{(ki)}}^2} & \dfrac{e_3^{(ki)}}{{e_3^{(ki)}}^2 + {e_4^{(ki)}}^2} & 0 & 0 & 0 & 0 \end{bmatrix}^{\mathrm{T}} \delta\mathbf{e}^{(ki)}\end{aligned} \tag{3.26}$$

The generalized external force due to the applied moment can be found by the following formula

$$\mathbf{Q}_e^{(ki)}\delta\mathbf{e}^{(ki)} = M\delta\alpha \tag{3.27}$$

Then it can be given as

$$\mathbf{Q}_e^{(ki)} = \begin{bmatrix} 0 & 0 & \dfrac{-Me_4^{(ki)}}{{e_3^{(ki)}}^2 + {e_4^{(ki)}}^2} & \dfrac{Me_3^{(ki)}}{{e_3^{(ki)}}^2 + {e_4^{(ki)}}^2} & 0 & 0 & 0 & 0 \end{bmatrix}^{\mathrm{T}} \qquad (3.28)$$

3.5. Connectivity of the Conventional Planar ANCF Beam Element

Let the body k be composed of two conventional planar ANCF beam elements as given in Figure 3.2.

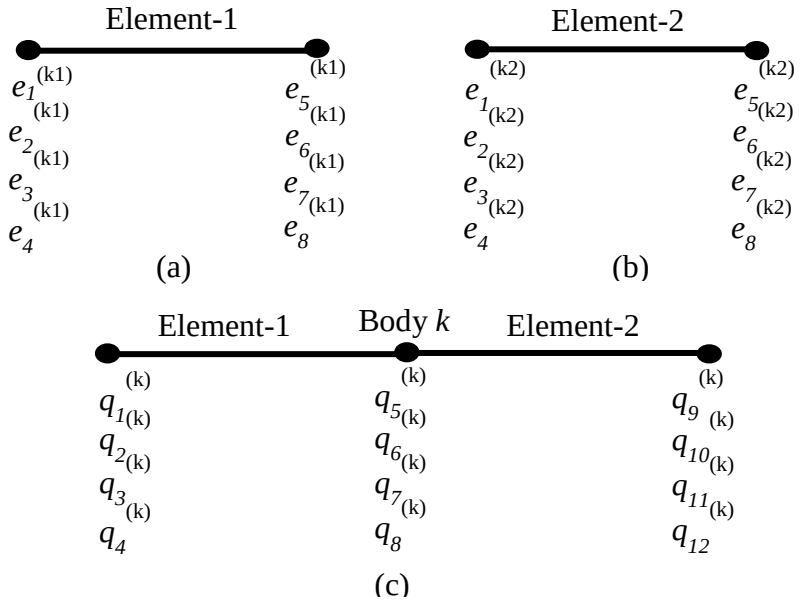

Figure 3.2 (a) Element-1, (b) Element-2 and (c) Body k

Nodal coordinates of Element 1, Element 2 and generalized coordinates of Body k are given as follows

$$\mathbf{e}^{(k1)} = \begin{bmatrix} e_1^{(k1)} & e_2^{(k1)} & e_3^{(k1)} & e_4^{(k1)} & e_5^{(k1)} & e_6^{(k1)} & e_7^{(k1)} & e_8^{(k1)} \end{bmatrix}^{\mathrm{T}} \qquad (3.29)$$

$$\mathbf{e}^{(k2)} = \begin{bmatrix} e_1{}^{(k2)} & e_2{}^{(k2)} & e_3{}^{(k2)} & e_4{}^{(k2)} & e_5{}^{(k2)} & e_6{}^{(k2)} & e_7{}^{(k2)} & e_8{}^{(k2)} \end{bmatrix}^{\mathrm{T}} \tag{3.30}$$

$$\mathbf{q}^{(k)} = [q_1{}^{(k)} \quad q_2{}^{(k)} \quad q_3{}^{(k)} \quad q_4{}^{(k)} \quad \cdots \quad q_{10}{}^{(k)} \quad q_{11}{}^{(k)} \quad q_{12}{}^{(k)}]^{\mathrm{T}} \tag{3.31}$$

Total number of nodal coordinates composed of i number of elements can be found as

$$n = 8 + 4(i-1) = 4(i+1) \tag{3.32}$$

The Boolean matrices have the dimension of 8 x n, and composed of zeros and ones to relate the elemental variables to the body variables. For example, the Boolean matrices for the Body k composed of two elements are given as follows

$$\mathbf{B}^{(k1)} = \begin{bmatrix} 1 & 0 & 0 & 0 & 0 & 0 & 0 & 0 & 0 & 0 & 0 & 0 \\ 0 & 1 & 0 & 0 & 0 & 0 & 0 & 0 & 0 & 0 & 0 & 0 \\ 0 & 0 & 1 & 0 & 0 & 0 & 0 & 0 & 0 & 0 & 0 & 0 \\ 0 & 0 & 0 & 1 & 0 & 0 & 0 & 0 & 0 & 0 & 0 & 0 \\ 0 & 0 & 0 & 0 & 1 & 0 & 0 & 0 & 0 & 0 & 0 & 0 \\ 0 & 0 & 0 & 0 & 0 & 1 & 0 & 0 & 0 & 0 & 0 & 0 \\ 0 & 0 & 0 & 0 & 0 & 0 & 1 & 0 & 0 & 0 & 0 & 0 \\ 0 & 0 & 0 & 0 & 0 & 0 & 0 & 1 & 0 & 0 & 0 & 0 \end{bmatrix} \tag{3.33}$$

$$\mathbf{B}^{(k2)} = \begin{bmatrix} 0 & 0 & 0 & 0 & 1 & 0 & 0 & 0 & 0 & 0 & 0 & 0 \\ 0 & 0 & 0 & 0 & 0 & 1 & 0 & 0 & 0 & 0 & 0 & 0 \\ 0 & 0 & 0 & 0 & 0 & 0 & 1 & 0 & 0 & 0 & 0 & 0 \\ 0 & 0 & 0 & 0 & 0 & 0 & 0 & 1 & 0 & 0 & 0 & 0 \\ 0 & 0 & 0 & 0 & 0 & 0 & 0 & 0 & 1 & 0 & 0 & 0 \\ 0 & 0 & 0 & 0 & 0 & 0 & 0 & 0 & 0 & 1 & 0 & 0 \\ 0 & 0 & 0 & 0 & 0 & 0 & 0 & 0 & 0 & 0 & 1 & 0 \\ 0 & 0 & 0 & 0 & 0 & 0 & 0 & 0 & 0 & 0 & 0 & 1 \end{bmatrix} \tag{3.34}$$

Then the vector of generalized coordinates can be found by using the vector of nodal coordinates and the Boolean matrices as

$$\mathbf{q}^{(k)} = \sum_i \mathbf{B}^{(ki)^{\mathrm{T}}} \mathbf{e}^{(ki)} \tag{3.35}$$

In the same manner, the mass matrix and the generalized force matrix for a body k can be determined as follows

$$\mathbf{M}^{(k)} = \sum_{i} \mathbf{B}^{(ki)^{\mathrm{T}}} \mathbf{M}^{(ki)} \mathbf{B}^{(ki)} \tag{3.36}$$

$$\mathbf{Q}^{(k)} = \sum_{i} \mathbf{B}^{(ki)^{\mathrm{T}}} \mathbf{Q}^{(ki)} \tag{3.37}$$

Then the mass matrix, the vector of generalized coordinates and the vector of generalized forces are given for a multibody system composed of N number of bodies as

$$\mathbf{M} = \begin{bmatrix} \mathbf{M}^{(1)} & \mathbf{0} & \mathbf{0} & \mathbf{0} & \cdots & \mathbf{0} \\ \mathbf{0} & \mathbf{M}^{(2)} & \mathbf{0} & \mathbf{0} & \ldots & \mathbf{0} \\ \mathbf{0} & \mathbf{0} & \mathbf{M}^{(3)} & \mathbf{0} & \ldots & \mathbf{0} \\ \mathbf{0} & \mathbf{0} & \mathbf{0} & \mathbf{M}^{(4)} & \ldots & \mathbf{0} \\ \vdots & \vdots & \vdots & \vdots & \ddots & \vdots \\ \mathbf{0} & \mathbf{0} & \mathbf{0} & \mathbf{0} & \ldots & \mathbf{M}^{(N)} \end{bmatrix} \tag{3.38}$$

$$\mathbf{Q} = [\mathbf{Q}^{(1)} \quad \mathbf{Q}^{(2)} \quad \mathbf{Q}^{(3)} \quad \mathbf{Q}^{(4)} \quad \ldots \quad \mathbf{Q}^{(N)}]^{\mathrm{T}} \tag{3.39}$$

$$\mathbf{q} = [\mathbf{q}^{(1)} \quad \mathbf{q}^{(2)} \quad \mathbf{q}^{(3)} \quad \mathbf{q}^{(4)} \quad \ldots \quad \mathbf{q}^{(N)}]^{\mathrm{T}} \tag{3.40}$$

CHAPTER 4

THE NEW PLANAR ANCF BEAM ELEMENT

A new planar beam element in ANCF is developed with different shape functions and element nodal systematics. Shape function matrix of the proposed element is derived from the quadratic Bernstein polynomials. With three nodes on the element, deformations and displacements can be described by six degrees of freedom. Two of these nodes are located at the initial and last material points on the element. The third node is a free node, and it does not have to be located on the material. At each node, there are two degrees of freedom that make totally six degrees of freedom in the element. The nodal degrees of freedom are the global coordinates so that neither angles, nor slopes are used as nodal variables. To define the orientation and deformed shape of the beam, the middle node is used.

The new element is iso-parametric, and it uses global coordinates similar to the conventional one. Also, the mass matrix is constant, and there are no centrifugal and Coriolis forces. Since the shape function polynomials are quadratic instead of cubic, and degrees of freedom are less than the conventional beam element type, the generalized elastic force vector is simplified considerably.

4.1. Bernstein Polynomials and Bézier Curves

Bernstein polynomials are first introduced by Sergei Natanovich Bernstein, and used in the mathematical field. Bernstein basis polynomials of degree n are given as follows [25]

$$b_{m,n}(x) = \binom{n}{m} x^m (1-x)^{n-m} \quad , m = 0,1,\dots,n \tag{4.1}$$

where $\binom{n}{m}$ is a binomial coefficient. A linear combination of the Bernstein basis polynomials gives a Bernstein polynomial of degree n as

$$B_n(x) = \sum_{m=0}^{n} \beta_m \, b_{m,n}(x) \tag{4.2}$$

Here β_m are the Bernstein coefficients. Bernstein basis polynomials of second degree are found from Equation (4.1) as

$$b_{0,2}(x) = (1-x)^2, \qquad b_{1,2}(x) = 2x(1-x), \qquad b_{2,2}(x) = x^2 \tag{4.3}$$

and they can be plotted for $0 \leq x \leq 1$ as in Figure 4.1.

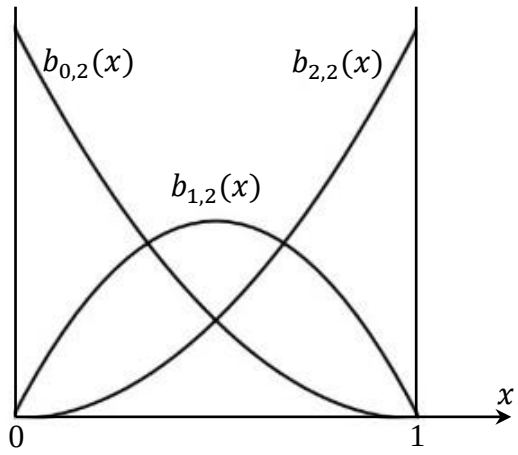

Figure 4.1 Bernstein basis polynomials.

A Bézier curve is a parametric curve which uses Bernstein basis polynomials. Also, Bézier surfaces can be obtained by the generalizations of Bézier curves to higher dimensions. Bézier curves are first used in the design of automobile bodies at Renault by the French engineer Pierre Bézier, who published his works in 1962.

Today Bézier curves and surfaces are widely used in computer graphics, games and also in computer-aided design (CAD) programs to describe complex geometries.

A set of control points is used to define a Bézier curve. First and last control points are located at the ends of a curve, and intermediate control points are used to describe the path of a smooth curve. Intermediate control points don't have to lie on the curve.

In this study, only quadratic Bézier curves are used and transformed into the finite element systematics. In quadratic Bézier curves, three control points exist, and a curve that is tangent to the lines between control points can be described parametrically by $\mathbf{B}(t)$ function where $t \in [0,1]$ so that $\mathbf{B}(0) = \mathbf{P}_0$ and $\mathbf{B}(1) = \mathbf{P}_2$. A quadratic Bézier curve and control points are given in Figure 4.2.

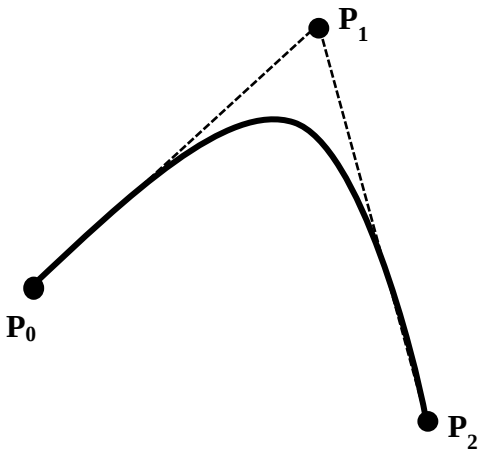

Figure 4.2 A quadratic Bézier curve and control points

The function of a quadratic Bézier curve can be given as follows

$$\mathbf{B}(t) = (1-t)^2\mathbf{P}_0 + 2t(1-t)\mathbf{P}_1 + t^2\mathbf{P}_2\,, \qquad t \in [0,1] \tag{4.4}$$

Note that the function is a special case of Bernstein polynomials of second degree where Bernstein coefficients are the positions of the control points.

4.2. Nodal Coordinates and Shape Function Matrix of the New Planar ANCF Beam Element

The new planar beam element in undeformed and deformed configurations is given in Figure 4.3. The global position vector of the beam element at an arbitrary point K is found by Equation (2.22). As can be seen in Figure 4.3, there are three nodes on the element, and the middle node is used to describe the orientation and the slope.

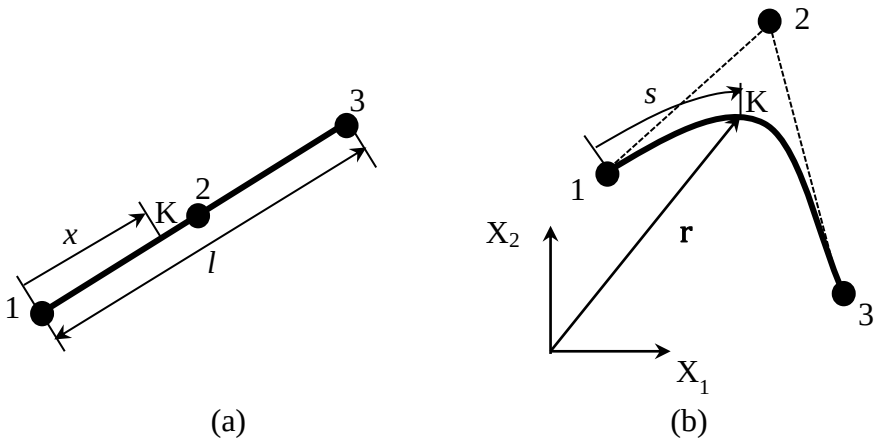

Figure 4.3 Undeformed (a) and deformed (b) configurations of the new planar ANCF beam element.

Shape functions of the element are composed of quadratic Bernstein basis polynomials. The shape function matrix are given as

$$\mathbf{S}^{(ki)} = \begin{bmatrix} (1-\xi)^2 & 0 & 2(1-\xi)\xi & 0 & \xi^2 & 0 \\ 0 & (1-\xi)^2 & 0 & 2(1-\xi)\xi & 0 & \xi^2 \end{bmatrix} \qquad (4.5)$$

where $\xi = x/l$, x is the coordinate of an arbitrary point on the element in undeformed configuration, and l is the length of the beam element.

There are totally six nodal coordinates in the element, and all of them are the global positions of the nodes. The vector of nodal coordinates of the element is given as below

$$\mathbf{e}^{(ki)} = \begin{bmatrix} e_1^{(ki)} & e_2^{(ki)} & e_3^{(ki)} & e_4^{(ki)} & e_5^{(ki)} & e_6^{(ki)} \end{bmatrix}^{\mathrm{T}} \tag{4.6}$$

where

$$\begin{aligned} e_1^{(ki)} &= {}^1r_{\mathrm{X}_1}^{(ki)}, \quad e_2^{(ki)} = {}^1r_{\mathrm{X}_2}^{(ki)}, \quad e_3^{(ki)} = {}^2r_{\mathrm{X}_1}^{(ki)}, \\ e_4^{(ki)} &= {}^2r_{\mathrm{X}_2}^{(ki)}, \quad e_5^{(ki)} = {}^3r_{\mathrm{X}_1}^{(ki)}, \quad e_6^{(ki)} = {}^3r_{\mathrm{X}_2}^{(ki)} \end{aligned} \tag{4.7}$$

4.3. Mass Matrix of the New Planar ANCF Beam Element

Using the vector of nodal coordinates and the shape function matrix for the new planar ANCF beam element, the mass matrix can be found explicitly by using Equation (2.25) as

$$\mathbf{M}^{(ki)} = m \begin{bmatrix} \frac{1}{5} & 0 & \frac{1}{10} & 0 & \frac{1}{30} & 0 \\ 0 & \frac{1}{5} & 0 & \frac{1}{10} & 0 & \frac{1}{30} \\ \frac{1}{10} & 0 & \frac{2}{15} & 0 & \frac{1}{10} & 0 \\ 0 & \frac{1}{10} & 0 & \frac{2}{15} & 0 & \frac{1}{10} \\ \frac{1}{30} & 0 & \frac{1}{10} & 0 & \frac{1}{5} & 0 \\ 0 & \frac{1}{30} & 0 & \frac{1}{10} & 0 & \frac{1}{5} \end{bmatrix} \tag{4.8}$$

4.4. Stiffness Matrices of the New Planar ANCF Beam Element

If E, A and I are assumed to be constant, stiffness matrices can be found by using Equations (3.6) and (3.17) using the shape function matrix and the vector of nodal coordinates of the new planar ANCF beam element.

If Equation (2.44) is used with $\mathbf{e_r} = [0 \quad 0 \quad l/2 \quad 0 \quad l \quad 0]^{\mathrm{T}}$, the longitudinal stiffness matrix can be written explicitly as

$$\mathbf{K}_{sl}^{(ki)} = \begin{bmatrix} K_{sl_1} & 0 & K_{sl_2} & 0 & K_{sl_3} & 0 \\ & K_{sl_1} & 0 & K_{sl_2} & 0 & K_{sl_3} \\ & & K_{sl_4} & 0 & K_{sl_5} & 0 \\ & & & K_{sl_4} & 0 & K_{sl_5} \\ & sym & & & K_{sl_6} & 0 \\ & & & & & K_{sl_6} \end{bmatrix} \tag{4.9}$$

where elements in the $\mathbf{K}_{sl}$ matrix are given as follows

$$\begin{aligned} K_{sl_1} = \frac{2EA}{15l^3}\Big[&12\left(e_1^{(ki)^2} + e_2^{(ki)^2}\right) - 18\left(e_1^{(ki)}e_3^{(ki)} + e_2^{(ki)}e_4^{(ki)}\right) \\ &- 6\left(e_1^{(ki)}e_5^{(ki)} + e_2^{(ki)}e_6^{(ki)}\right) + 8\left(e_3^{(ki)^2} + e_4^{(ki)^2}\right) \\ &+ 2\left(e_3^{(ki)}e_5^{(ki)} + e_4^{(ki)}e_6^{(ki)}\right) + 8\left(e_5^{(ki)^2} + e_6^{(ki)^2}\right) - 5l^2\Big] \end{aligned} \tag{4.10}$$

$$\begin{aligned} K_{sl_2} = \frac{EA}{15l^3}\Big[&-18\left(e_1^{(ki)^2} + e_2^{(ki)^2}\right) + 32\left(e_1^{(ki)}e_3^{(ki)} + e_2^{(ki)}e_4^{(ki)}\right) \\ &+ 4\left(e_1^{(ki)}e_5^{(ki)} + e_2^{(ki)}e_6^{(ki)}\right) - 12\left(e_3^{(ki)^2} + e_4^{(ki)^2}\right) \\ &- 8\left(e_3^{(ki)}e_5^{(ki)} + e_4^{(ki)}e_6^{(ki)}\right) + 2\left(e_5^{(ki)^2} + e_6^{(ki)^2}\right) + 5l^2\Big] \end{aligned} \tag{4.11}$$

$$\begin{aligned} K_{sl_3} = \frac{EA}{15l^3}\Big[&-6\left(e_1^{(ki)^2} + e_2^{(ki)^2}\right) + 4\left(e_1^{(ki)}e_3^{(ki)} + e_2^{(ki)}e_4^{(ki)}\right) \\ &+ 8\left(e_1^{(ki)}e_5^{(ki)} + e_2^{(ki)}e_6^{(ki)}\right) - 4\left(e_3^{(ki)^2} + e_4^{(ki)^2}\right) \\ &+ 4\left(e_3^{(ki)}e_5^{(ki)} + e_4^{(ki)}e_6^{(ki)}\right) - 6\left(e_5^{(ki)^2} + e_6^{(ki)^2}\right) + 5l^2\Big] \end{aligned} \tag{4.12}$$

$$K_{sl_4} = \frac{2EA}{15l^3}\Big[-8\left(e_1^{(ki)^2} + e_2^{(ki)^2}\right) + 12\left(e_1^{(ki)}e_3^{(ki)} + e_2^{(ki)}e_4^{(ki)}\right) + 4\left(e_1^{(ki)}e_5^{(ki)} + e_2^{(ki)}e_6^{(ki)}\right) - 12\left(e_3^{(ki)^2} + e_4^{(ki)^2}\right) + 12\left(e_3^{(ki)}e_5^{(ki)} + e_4^{(ki)}e_6^{(ki)}\right) - 8\left(e_5^{(ki)^2} + e_6^{(ki)^2}\right) + 5l^2\Big] \tag{4.13}$$

$$K_{sl_5} = \frac{EA}{15l^3}\Big[2\left(e_1^{(ki)^2} + e_2^{(ki)^2}\right) - 8\left(e_1^{(ki)}e_3^{(ki)} + e_2^{(ki)}e_4^{(ki)}\right) + 4\left(e_1^{(ki)}e_5^{(ki)} + e_2^{(ki)}e_6^{(ki)}\right) - 12\left(e_3^{(ki)^2} + e_4^{(ki)^2}\right) + 32\left(e_3^{(ki)}e_5^{(ki)} + e_4^{(ki)}e_6^{(ki)}\right) - 18\left(e_5^{(ki)^2} + e_6^{(ki)^2}\right) + 5l^2\Big] \tag{4.14}$$

$$K_{sl_6} = \frac{2EA}{15l^3}\Big[2\left(e_1^{(ki)^2} + e_2^{(ki)^2}\right) + 2\left(e_1^{(ki)}e_3^{(ki)} + e_2^{(ki)}e_4^{(ki)}\right) - 6\left(e_1^{(ki)}e_5^{(ki)} + e_2^{(ki)}e_6^{(ki)}\right) + 8\left(e_3^{(ki)^2} + e_4^{(ki)^2}\right) - 18\left(e_3^{(ki)}e_5^{(ki)} + e_4^{(ki)}e_6^{(ki)}\right) + 12\left(e_5^{(ki)^2} + e_6^{(ki)^2}\right) + 5l^2\Big] \tag{4.15}$$

By using Equation (3.17), the transverse stiffness matrix can be given explicitly as

$$\mathbf{K}_{st}^{(ki)} = \frac{4EI}{l^3}\begin{bmatrix} 1 & 0 & -2 & 0 & 1 & 0 \\ & 1 & 0 & -2 & 0 & 1 \\ & & 4 & 0 & -2 & 0 \\ & & & 4 & 0 & -2 \\ & sym & & & 1 & 0 \\ & & & & & 1 \end{bmatrix} \tag{4.16}$$

4.5. Generalized External Forces for the New Planar ANCF Beam Element

For the gravitational force $\mathbf{F}_g = mg\mathbf{u}$ where $\mathbf{u}$ is the unit vector along the gravitational direction with respect to the global coordinate system, and g is the gravitational acceleration; the generalized external force due to the gravitation can be

found explicitly by using Equation (2.58) for the new planar ANCF beam element as follows

$$\mathbf{Q}_e^{(ki)} = mg\begin{bmatrix} \frac{1}{2} & 0 & \frac{l}{12} & 0 & \frac{1}{2} & 0 & -\frac{l}{12} & 0 \\ 0 & \frac{1}{2} & 0 & \frac{l}{2} & 0 & \frac{1}{2} & 0 & -\frac{l}{12} \end{bmatrix}^{\mathrm{T}} \mathbf{u} \tag{4.17}$$

The moment, M, is assumed to act on a cross-section of the beam at the initial node as can be seen in Figure 4.4. Virtual angle change, $\delta\alpha$, is assumed as a result of the bending moment, M, and it can be given as follows

$$\delta\alpha = \delta\left[\tan^{-1}\left(\frac{e_2^{(ki)} - e_4^{(ki)}}{e_1^{(ki)} - e_3^{(ki)}}\right)\right] \tag{4.18}$$

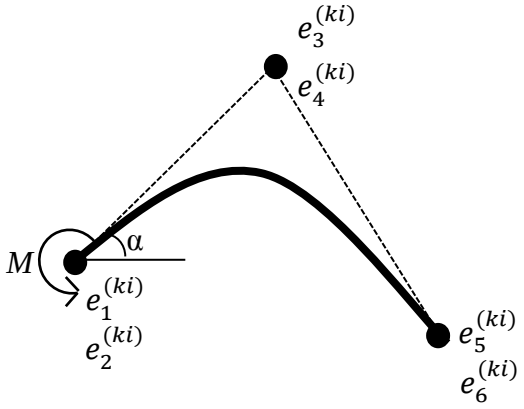

Figure 4.4 The new planar beam element under the effect of bending forces.

Then the generalized external force due to the bending is determined by using Equations (3.20) and (4.18) as

$$\mathrm{M}\delta\alpha = \mathrm{M}\delta\left[\tan^{-1}\left(\frac{e_2^{(ki)} - e_4^{(ki)}}{e_1^{(ki)} - e_3^{(ki)}}\right)\right] = \mathbf{Q}_e^{(ki)}\delta\mathbf{e}^{(ki)} \tag{4.19}$$

It can be also given in the matrix form as follows

$$\mathbf{Q}_e^{(ki)} = [Q_{e_1} \quad Q_{e_2} \quad Q_{e_3} \quad Q_{e_4} \quad 0 \quad 0]^{\mathrm{T}} \tag{4.20}$$

where the elements in the above vector are

$$Q_{e_1} = \frac{-(e_2^{(ki)} - e_4^{(ki)})}{(e_1^{(ki)} - e_3^{(ki)})^2\left[\frac{\left(e_2^{(ki)} - e_4^{(ki)}\right)^2}{\left(e_1^{(ki)} - e_3^{(ki)}\right)^2} + 1\right]} \tag{4.21}$$

$$Q_{e_2} = \frac{1}{(e_1^{(ki)} - e_3^{(ki)})\left[\frac{\left(e_2^{(ki)} - e_4^{(ki)}\right)^2}{\left(e_1^{(ki)} - e_3^{(ki)}\right)^2} + 1\right]} \tag{4.22}$$

$$Q_{e_3} = \frac{(e_2^{(ki)} - e_4^{(ki)})}{(e_1^{(ki)} - e_3^{(ki)})^2\left[\frac{\left(e_2^{(ki)} - e_4^{(ki)}\right)^2}{\left(e_1^{(ki)} - e_3^{(ki)}\right)^2} + 1\right]} \tag{4.23}$$

$$Q_{e_4} = \frac{-1}{(e_1^{(ki)} - e_3^{(ki)})\left[\frac{\left(e_2^{(ki)} - e_4^{(ki)}\right)^2}{\left(e_1^{(ki)} - e_3^{(ki)}\right)^2} + 1\right]} \tag{4.24}$$

4.6. Connectivity of the New Planar ANCF Beam Element

End nodes of two consecutive elements can be connected with the similar procedure explained for the conventional planar ANCF beam element. Here again, the Boolean matrices are used for the connection.

It should be noted that continuity of the slopes of two consecutive elements should be satisfied. For this purpose, an additional constraint equation is introduced for the new planar ANCF beam element. In Figure 4.5, two connected elements are represented. For the continuity of the slopes at the connected ends of the beam elements, the following equation should be satisfied

$$\frac{\left(q_6{}^{(k)} - q_4{}^{(k)}\right)}{\left(q_5{}^{(k)} - q_3{}^{(k)}\right)} = \frac{\left(q_6{}^{(k)} - q_8{}^{(k)}\right)}{\left(q_5{}^{(k)} - q_7{}^{(k)}\right)} \tag{4.25}$$

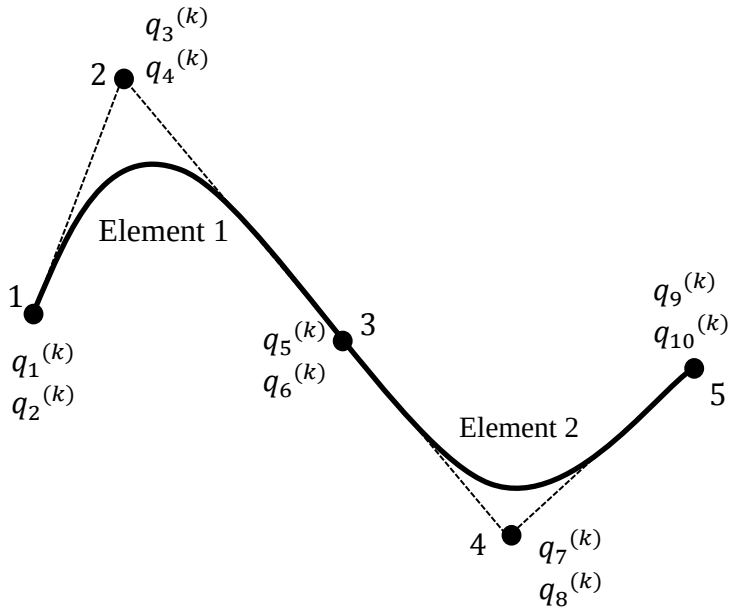

Figure 4.5 Connected two consecutive new planar ANCF beam elements

Taking second time derivative of Equation (4.25) yields the additional constraint equation as follows

$$\begin{aligned}\ddot{q}_3^{(k)}\left(q_6{}^{(k)} - q_8{}^{(k)}\right) + \ddot{q}_4^{(k)}\left(-q_5{}^{(k)} + q_7{}^{(k)}\right) + \ddot{q}_5^{(k)}\left(-q_4{}^{(k)} + q_8{}^{(k)}\right) \\ + \ddot{q}_6^{(k)}\left(-q_7{}^{(k)} + q_3{}^{(k)}\right) + \ddot{q}_7^{(k)}\left(-q_6{}^{(k)} + q_4{}^{(k)}\right) \\ + \ddot{q}_8^{(k)}\left(q_5{}^{(k)} - q_3{}^{(k)}\right) \\ = -2\dot{q}_5^{(k)}\dot{q}_8^{(k)} - 2\dot{q}_3^{(k)}\dot{q}_6^{(k)} - 2\dot{q}_3^{(k)}\dot{q}_8^{(k)} - 2\dot{q}_4^{(k)}\dot{q}_5^{(k)} \\ - 2\dot{q}_6^{(k)}\dot{q}_7^{(k)} - 2\dot{q}_7^{(k)}\dot{q}_4^{(k)}\end{aligned} \tag{4.26}$$

CHAPTER 5

NUMERICAL SOLUTION PROCEDURE

The equations of motion that are used in the analysis of a multibody system consist of a set of ordinary differential and algebraic equations. Solutions of differential algebraic equations (DAEs) are not straight forward as ordinary differential equations (ODEs). Three different approaches are proposed for the solution of DAEs namely as the direct integration method, the generalized coordinates partitioning method and the constraint stabilization method [17].

In the direct integration method, numerical integration methods of ODEs are used to integrate DAEs without any modification of equations or algorithms. The approach is easy to implement and computationally fast. However, constraint equations in the equations of motion are not ordinary differential equations, and solution procedure may cause some problems in the error control on the constraints [17].

The generalized coordinates partitioning method, also called as Wehage's partitioning technique, is proposed by Wehage and Haug [18]. In this technique, generalized coordinates are partitioned to dependent and independent coordinates. By using the Newton-Raphson method, constraint equations are solved to obtain dependent coordinates. Only independent coordinates are integrated so that error control is improved in this technique [17].

Last method is the constraint stabilization method proposed by Baumgarte [19]. This method is used to stabilize direct integration algorithms by adding the velocity and position terms of the constraint equations into the second derivative of the constraint equations. The method is fast and accurate but may lead to erroneous results by selecting improper coefficients of velocity and position terms [17].

In the direct integration, explicit and implicit integration methods are used. Explicit integration methods solve the dynamic equations of the system by using the variables at the current time step, while implicit methods find the solution by using the variables at both current and following time steps. Explicit methods can be said conditionally stable when

$$\Delta t < \frac{\alpha}{\omega_{max}} \tag{5.1}$$

where Δt is a time step size, α is a constant and ω_{max} is the highest frequency of the system. In the multibody systems, in which small numbers of degrees of freedom are used, the highest frequency of the system is not large, and time steps that can lead stable analysis may be reasonable [20].

In the multibody systems having highly deformable bodies, deformation modes can be associated with high frequencies, and the systems may have large numbers of degrees of freedom. As the frequency increases, explicit integrator must select smaller step-sizes to capture the oscillations in the solution. In this case, explicit integration methods can be very inefficient or even fail [21].

In fact, high-frequency oscillations are negligible in the solution, and since implicit methods do not trace high-frequency oscillations; they give better results with larger step times in many multibody system applications when compared to the explicit methods.

The implicit Newmark method, which is a numerical integration method used for the solution of structural dynamic problems [22], can be used conveniently in the solution of multibody systems that have highly deformable bodies. Some of the advantages of the Newmark method can be stated as [23]

- The resulting second order ODEs do not have to be reduced to the first order that leads smaller dimension of problems.
- The method has good stability properties.

- The amount of damping introduced to the system can be adjusted.

On the other hand, in the case of high numerical damping introduced to the system, accuracy of the solution may be affected. Improved methods, like Hilber-Hughes-Taylor (HHT) method, exist in the literature to diminish unwanted effects of damping on the accuracy of the solution [24].

Since dynamic equations are the form of DAEs due to the kinematic constraints, the Newmark method that is explained below is a modified version from the originally proposed one.

Let $\mathbf{q}$ be the generalized vector of coordinates, $\dot{\mathbf{q}}$ be the generalized vector of velocities, and $\ddot{\mathbf{q}}$ be the generalized vector of accelerations. Then, the Newmark integration equations depend on two integration parameters, β and γ, as

$$\mathbf{q}_{t+\Delta t} = \mathbf{q}_t + \Delta t\dot{\mathbf{q}}_t + \frac{\Delta t^2}{2}[(1-2\beta)\ddot{\mathbf{q}}_t + 2\beta\ddot{\mathbf{q}}_{t+\Delta t}] \tag{5.2}$$

$$\dot{\mathbf{q}}_{t+\Delta t} = \dot{\mathbf{q}}_t + \Delta t[(1-\gamma)\ddot{\mathbf{q}}_t + \gamma\ddot{\mathbf{q}}_{t+\Delta t}] \tag{5.3}$$

where Δt is the time step size, the subscripts t and $t+\Delta t$ denote variables at the current time and the following time steps.

Equations (5.2) and (5.3) can be used to discretize the equations of motion of the multibody system as follows

$$\begin{bmatrix} \mathbf{M} & \mathbf{C}_{\mathbf{q}_{t+\Delta t}}{}^{T} \\ \mathbf{C}_{\mathbf{q}_{t+\Delta t}} & \mathbf{0} \end{bmatrix} \begin{bmatrix} \ddot{\mathbf{q}}_{t+\Delta t} \\ \boldsymbol{\lambda}_{t+\Delta t} \end{bmatrix} = \begin{bmatrix} \mathbf{Q}_{t+\Delta t} \\ \boldsymbol{H}_{t+\Delta t} \end{bmatrix} \tag{5.4}$$

Since $\mathbf{q}_{t+\Delta t}$ and $\dot{\mathbf{q}}_{t+\Delta t}$ in the equations are functions of $\ddot{\mathbf{q}}_{t+\Delta t}$, unknowns in the Equation (5.4) become $\ddot{\mathbf{q}}_{t+\Delta t}$ and $\boldsymbol{\lambda}_{t+\Delta t}$.

Integration constants that are used to control the stability and the amount of damping introduced into the system should satisfy the following conditions

$$\gamma \geq \frac{1}{2} \quad , \quad \beta \geq \frac{\left(\gamma + \frac{1}{2}\right)^2}{4} \tag{5.5}$$

If γ value equals to 0.5, then there is no damping in the system. For higher γ values, numerical damping is introduced. If γ value equals to 0.5 and β value equals to 0.25, method returns to the trapezoidal method.

After using Equations (5.2) and (5.3); Equation (5.4) becomes a non-linear set of equations that depends on $\ddot{\mathbf{q}}_{t+\Delta t}$ and $\boldsymbol{\lambda}_{t+\Delta t}$. To evaluate this set of non-linear equations, the Newton-Raphson method can be used.

The Newton-Raphson method is a widely used root finding method. Consider a non-linear set of equations that has equal numbers of equations and unknowns as

$$\mathbf{F}(\mathbf{x}) = \mathbf{0} \tag{5.6}$$

where **x** is the vector of unknowns. Using the Taylor series, Equation (5.6) is written as

$$\mathbf{F}(\mathbf{x} + \boldsymbol{\delta}\mathbf{x}) = \mathbf{F}(\mathbf{x}) + \frac{\partial \mathbf{F}(\mathbf{x})}{\partial \mathbf{x}} \delta\mathbf{x} + O(\delta\mathbf{x}^2) \tag{5.7}$$

Jacobian matrix can be defined for the partial differential equations in Equation (5.7) as follows

$$\mathbf{J}(\mathbf{x}) = \frac{\partial \mathbf{F}(\mathbf{x})}{\partial \mathbf{x}} = \begin{bmatrix} \frac{\partial F_1}{\partial x_1} & \frac{\partial F_1}{\partial x_2} & \cdots & \frac{\partial F_1}{\partial x_n} \\ \frac{\partial F_2}{\partial x_1} & \frac{\partial F_2}{\partial x_2} & \cdots & \frac{\partial F_2}{\partial x_n} \\ \vdots & \vdots & \ddots & \vdots \\ \frac{\partial F_n}{\partial x_1} & \frac{\partial F_n}{\partial x_2} & \cdots & \frac{\partial F_n}{\partial x_n} \end{bmatrix} \tag{5.8}$$

Neglecting higher order terms in the Taylor series, and setting $\mathbf{F}(\mathbf{x}+\boldsymbol{\delta}\mathbf{x})=\mathbf{0}$, Equation (5.7) yields

$$\boldsymbol{\delta}\mathbf{x} = -\mathbf{J}^{-1}(\mathbf{x})\mathbf{F}(\mathbf{x}) \tag{5.9}$$

that means, each function approaches to zero together with the corrections $\boldsymbol{\delta}\mathbf{x}$. By using the corrections, updated value of the unknowns can be found as

$$\mathbf{x}^{n+1} = \mathbf{x}^{n} + \boldsymbol{\delta}\mathbf{x} = \mathbf{x}^{n} - \mathbf{J}^{-1}(\mathbf{x}^{n})\mathbf{F}(\mathbf{x}^{n}) \tag{5.10}$$

where $\mathbf{x}^{n}$ is the value of the vector of unknowns in the previous iteration, and $\mathbf{x}^{n+1}$ is the value of the vector of unknowns in the current iteration. This equation can be used iteratively until the specified error that is acceptable for the solution is reached. Error criterion [11] that is given below can be used for the iterative solutions as

$$\frac{\|\mathbf{x}^{n+1}-\mathbf{x}^{n}\|}{\|\mathbf{x}^{n+1}\|} < error \tag{5.11}$$

where the Euclidean norm is given as follows

$$\|\mathbf{x}\| = \sqrt{{x_1}^2 + {x_2}^2 + \cdots + {x_n}^2} \tag{5.12}$$

Therefore, the Newton-Raphson method can be used to determine unknowns $\ddot{\mathbf{q}}_{t+1}$ and $\boldsymbol{\lambda}_{t+1}$ starting with initial guesses. Initial guesses can be set with the initial conditions and initial configurations of the system for the first step.

Once $\ddot{\mathbf{q}}_{t+\Delta t}$ is determined, $\dot{\mathbf{q}}_{t+\Delta t}$ and $\mathbf{q}_{t+\Delta t}$ can be found from Equations (5.2) and (5.3). This procedure should be continued until the time reaches to the specified value. Computational algorithm based on the above procedure can be given as follows:

i. Input the beam properties, integration constants, step size, and total time of the analysis with other parameters.

ii. Solve the equations of motion for the initial conditions to get initial values of unknowns.

iii. Increase time step by Δt to find the solution at time $t+\Delta t$ by using the values at time t Use the Newmark method for expressing the generalized coordinates and the velocities in terms of the generalized accelerations.

iv. Start iteration loop to solve the set of non-linear equations for the generalized acceleration and Lagrange multipliers by using the Newton-Raphson method at each time step. Continue to solve the loops until error reaches to the specified value.

v. Calculate the generalized velocities and coordinates by using the Newmark equations for the next time step. Find and record the kinetic energies, strain energies and potential energies by using the generalized coordinates.

vi. To continue the analysis until time reaches to the specified value, go to step iii.

To analyze the flexible multibody problems by the absolute nodal coordinate formulation, codes are developed based on the above algorithm, and integrated to the MATLAB® software.

CHAPTER 6

COMPARISON OF THE NEW BEAM ELEMENT AND THE CONVENTIONAL ANCF BEAM ELEMENT

To compare the performance of the new planar ANCF (6-DOF-ANCF) beam element and the conventional planar ANCF (8-DOF-ANCF) beam element types, numerical results are given in this chapter. Two case studies are examined: the free-falling pendulum and the four-bar mechanism with a highly elastic coupler.

6.1. Free Falling Pendulum

Flexible pendulum that is examined here is attached by a pin joint at one end to the fixed frame, and the other end is set free. Parameters used in the analyses of the pendulum are given in Table 6.1.

Table 6.1 Parameters used in the analyses of the pendulum.

Mass [kg]	Length [mm]	Cross Sectional Area [mm^2]	Second Moment of Area [mm^4]	Modulus of Elasticity [GPa]
11.8	1000	1.96×10^3	3.07×10^5	1×10^{-3}

The pendulum is divided into four and ten finite elements, and the Newmark method is used in the solutions with a γ value of 0.6 and a β value of 0.3025. Maximum error and iteration numbers are selected as 0.001 and 50 respectively. Total analysis time is selected as 1 second with a time step of 0.01 seconds. The vertical tip position

of the pendulum is given in Figure 6.1. Also, simulation results of the free falling pendulum can be seen in Figure 6.2.

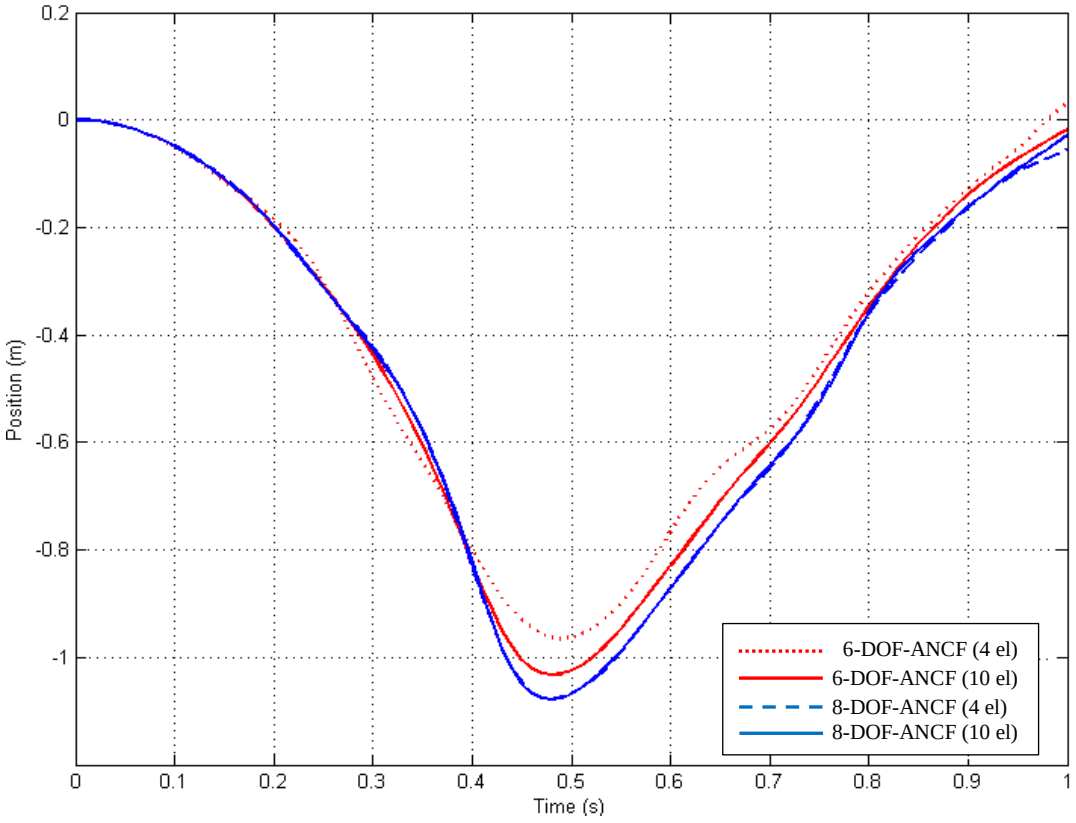

Figure 6.1 The vertical tip position of the free falling pendulum.

The total energy of the free falling pendulum is composed of the potential energy, the kinetic energy and the strain energy. Since there is no energy input or output in the system, it is expected that energy is conserved throughout the analyses. Energy graphs of the pendulum are given in Figure 6.3. Reference is selected at the initial position so that the potential energy is zero. The kinetic and the strain energies are also zero initially.

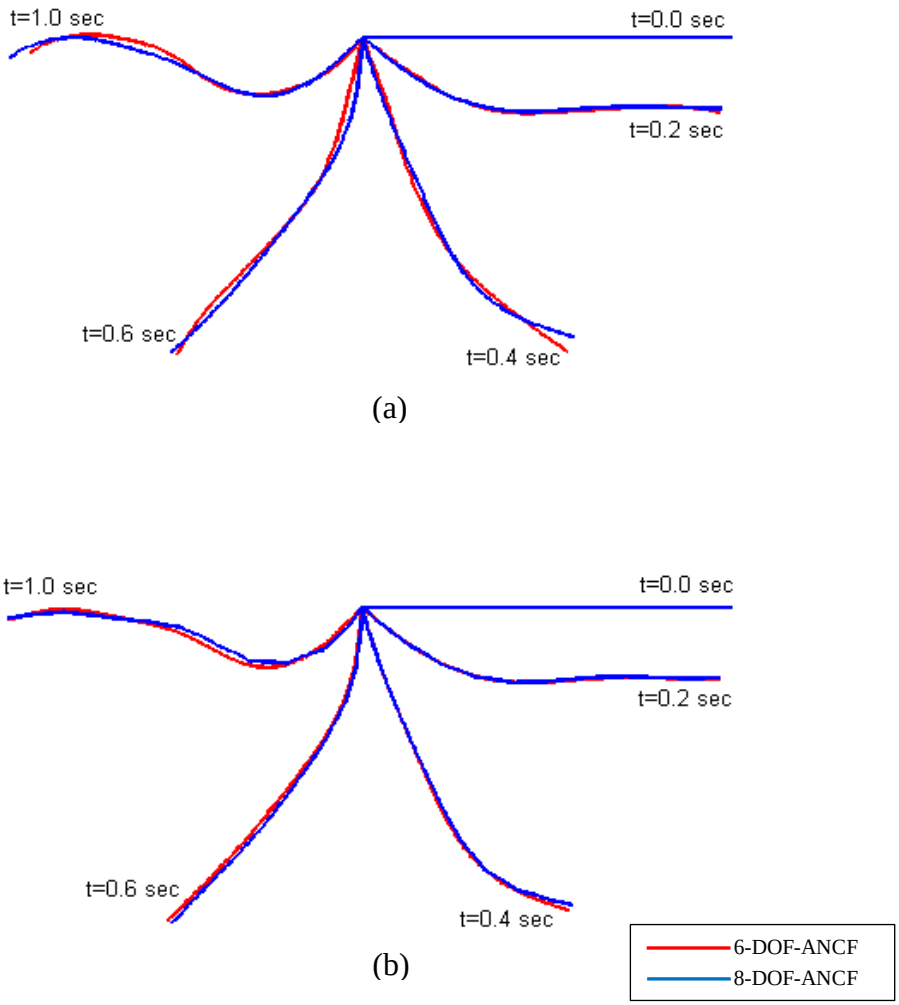

Figure 6.2 Simulations of the free falling pendulum with: (a) 4 elements, (b) 10 elements.

It can be seen that results are close to each other for both element types. Especially when element numbers are increased to ten, results are almost same.

In Table 6.2, CPU time ratios are given with respect to the 6-DOF-ANCF beam element type with four elements. Although accuracies are close to each other, computational time is reduced considerably when the 6-DOF-ANCF beam element type is used.

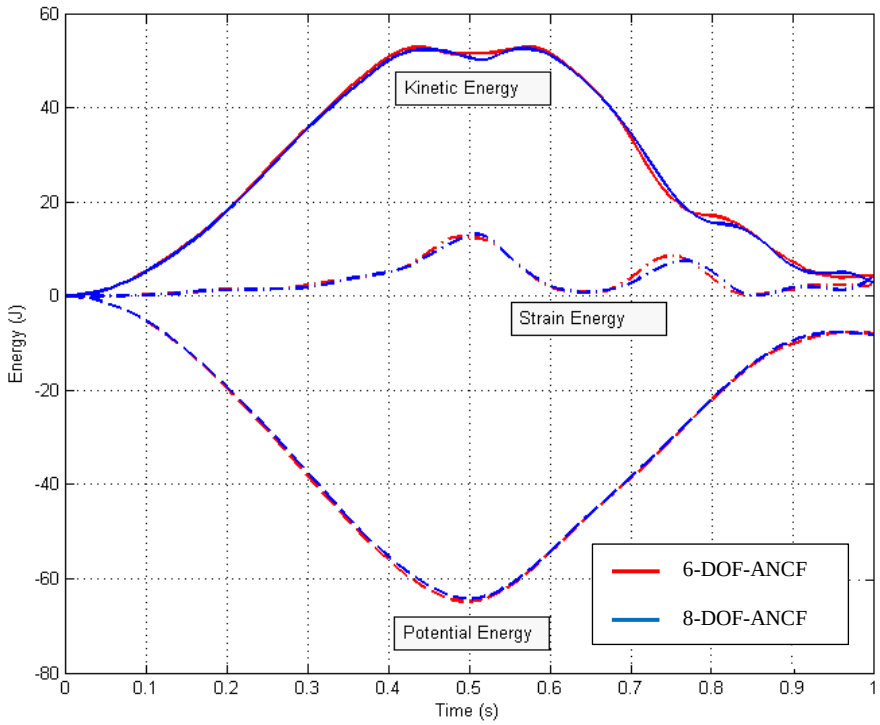

(a)

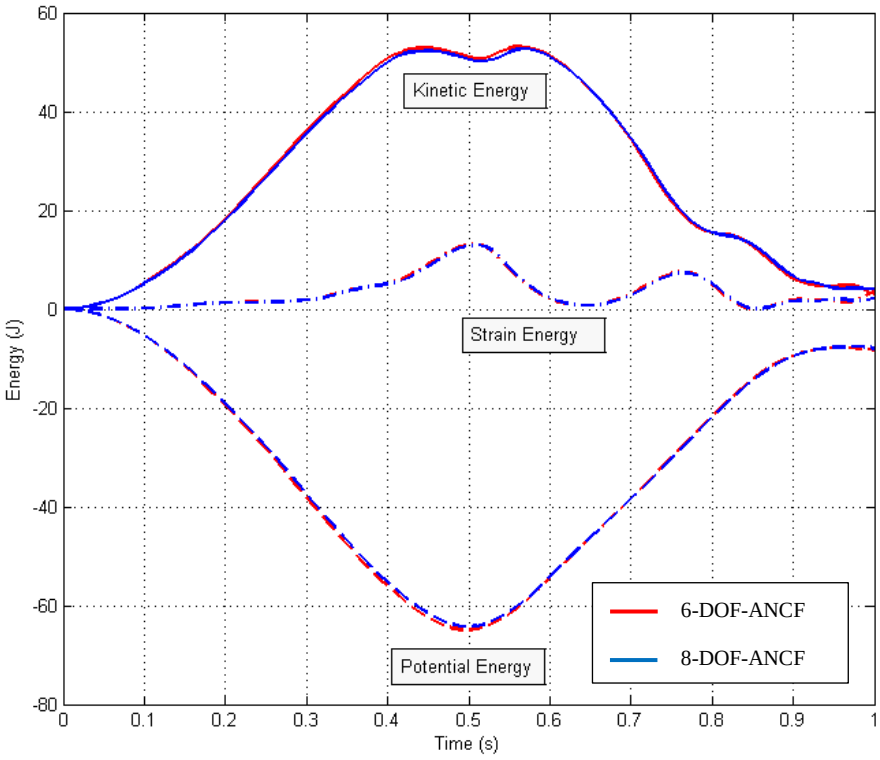

(b)

Figure 6.3 Energy balance of the pendulum for: (a) 4 elements, (b) 10 elements.

Table 6.2 CPU time ratios of the pendulum

	4 Elements	10 Elements
6-DOF-ANCF	1	2.42
8-DOF-ANCF	3.13	8.26

6.2. Flexible Four-Bar Mechanism with Highly Elastic Coupler

Four-bar mechanism shown in Figure 6.4 has three links: a crank, a coupler and a follower. The mechanism is under the gravity effect, and is driven by the moment applied to the crank. The variation of the applied moment is given in Figure 6.5.

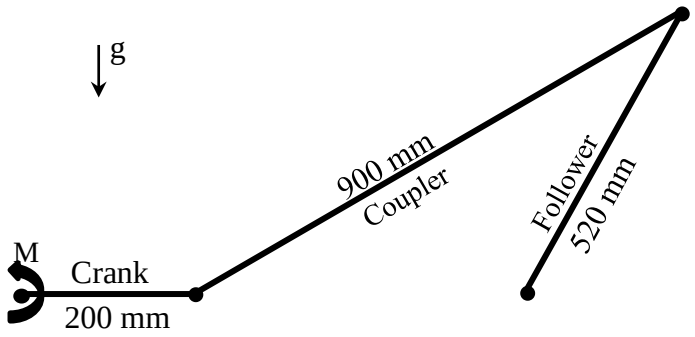

Figure 6.4 Four-bar mechanism with highly elastic coupler.

Six models are studied with different element numbers and different element types as given in Table 6.3.

The crank is selected to have a higher rigidity as compared to the other links, and the coupler is highly flexible so that very large deformations can be observed.

Parameters of the links are given in Table 6.4. Here the properties, the cases and the other parameters are taken from the study of Berzeri et al. [5].

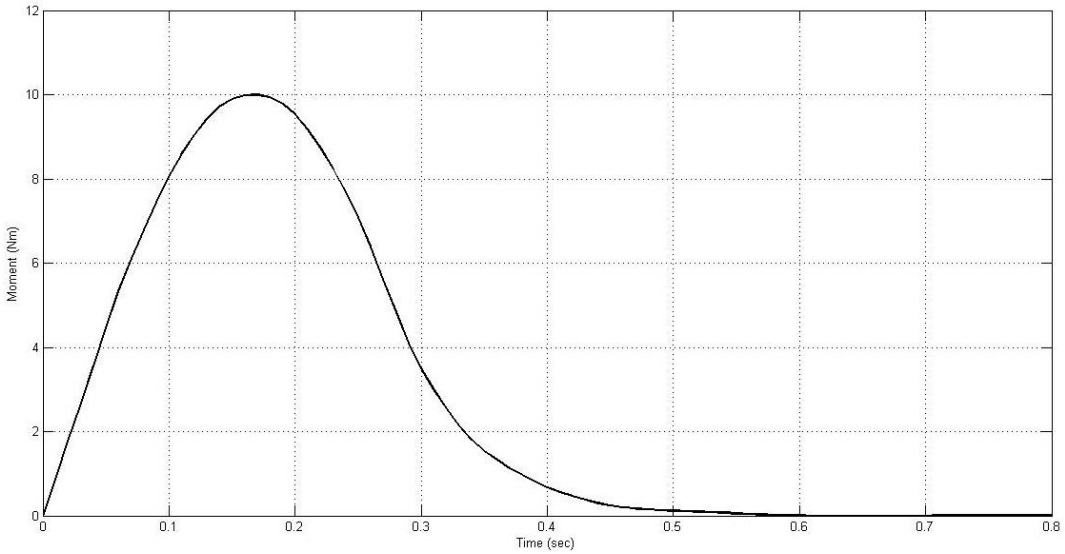

Figure 6.5 Applied moment versus time graph [5].

Table 6.3 Model names and element numbers of the links.

	Crank	Coupler	Follower
6-DOF-ANCF (6 el) 8-DOF-ANCF (6 el)	1	6	4
6-DOF-ANCF (9 el) 8-DOF-ANCF (9 el)	1	9	4
6-DOF-ANCF (15 el) 8-DOF-ANCF (15 el)	1	15	4

Table 6.4 Parameters of four-bar mechanism with highly elastic coupler [5].

	Mass [kg]	Cross Sectional Area [mm^2]	Second Moment of Area [mm^4]	Modulus of Elasticity [GPa]
Crank	0.68	1.3×10^3	1.3×10^5	1.0
Coupler	2.47	2.0×10^3	3.1×10^5	5×10^{-3}
Follower	1.47	7.1×10^2	4.0×10^4	0.5

In the solution, maximum error and iteration numbers are selected as 1×10^{-3} and 75. Total analysis time is chosen as 0.8 seconds with a time step of 0.01 seconds. The transverse mid-point deflection graph and the strain energy graph of the coupler are given in Figure 6.6 and Figure 6.7, respectively.

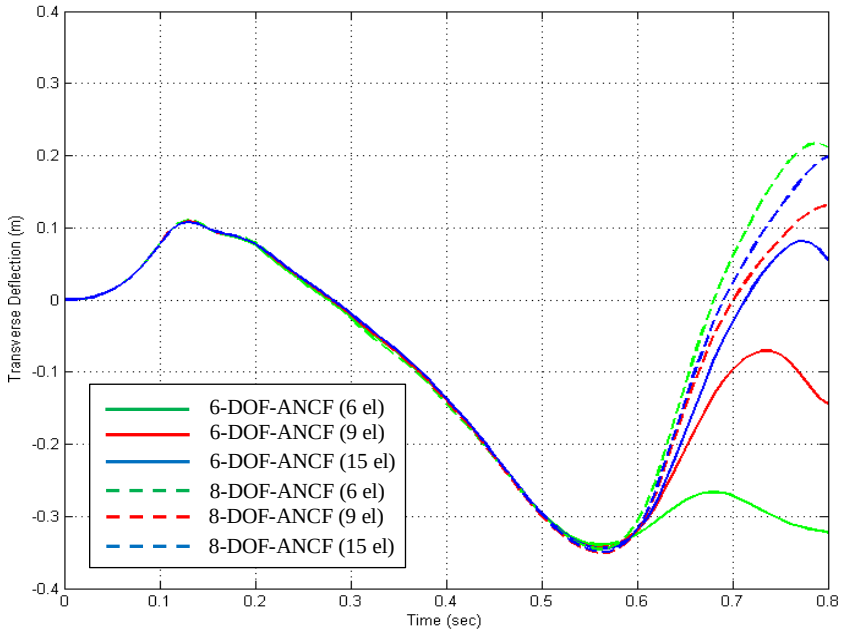

Figure 6.6 Transverse mid-point deflection of the coupler.

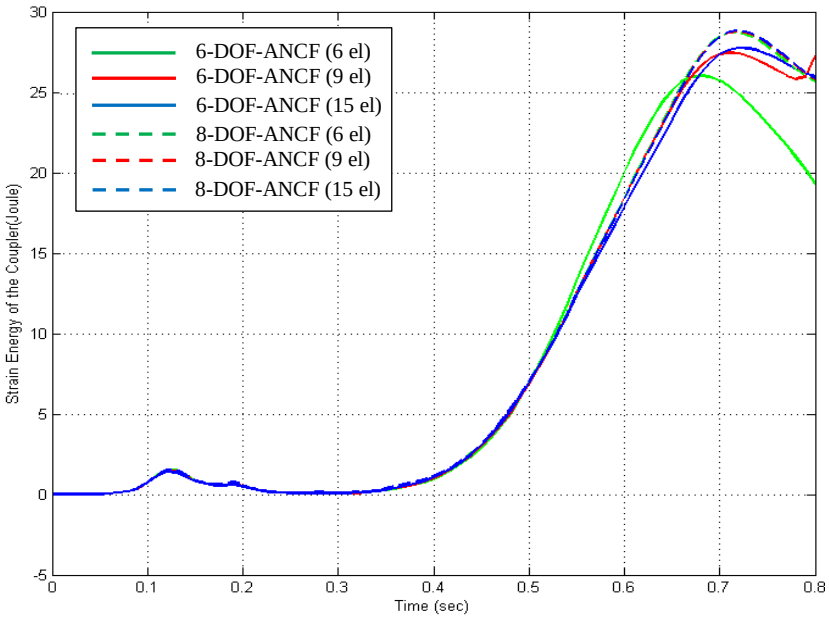

Figure 6.7 Strain energy of the coupler.

The simulation results are shown in Figures 6.8, 6.9 and 6.10 for different number of elements.

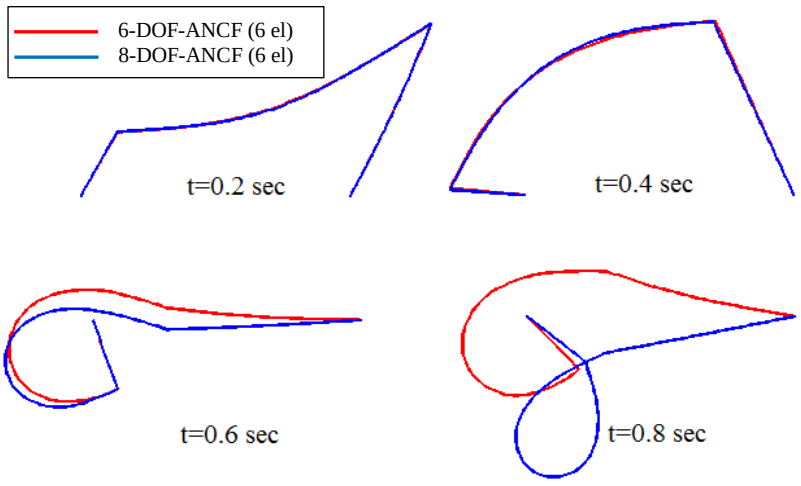

Figure 6.8 Simulation of the four-bar mechanism using 6 elements in the coupler.

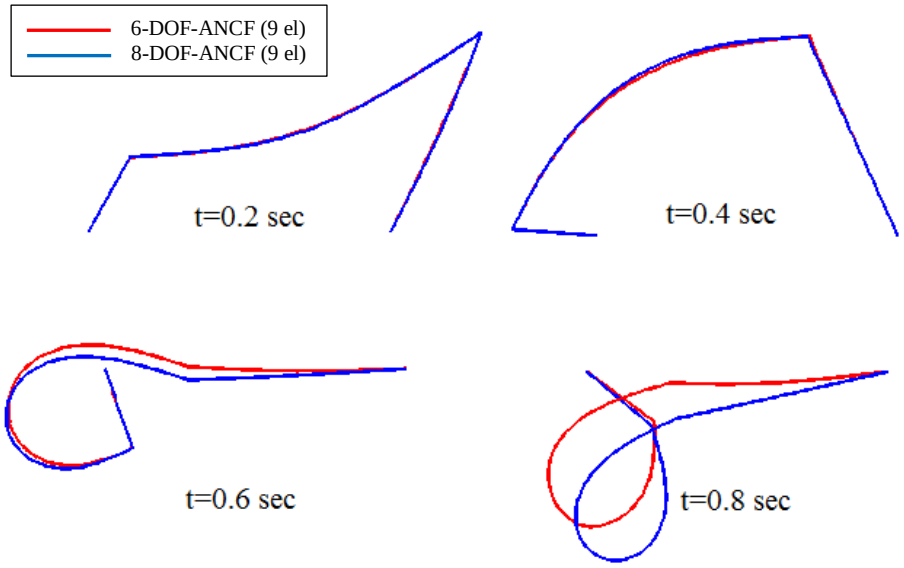

Figure 6.9 Simulation of the four-bar mechanism using 9 elements in the coupler.

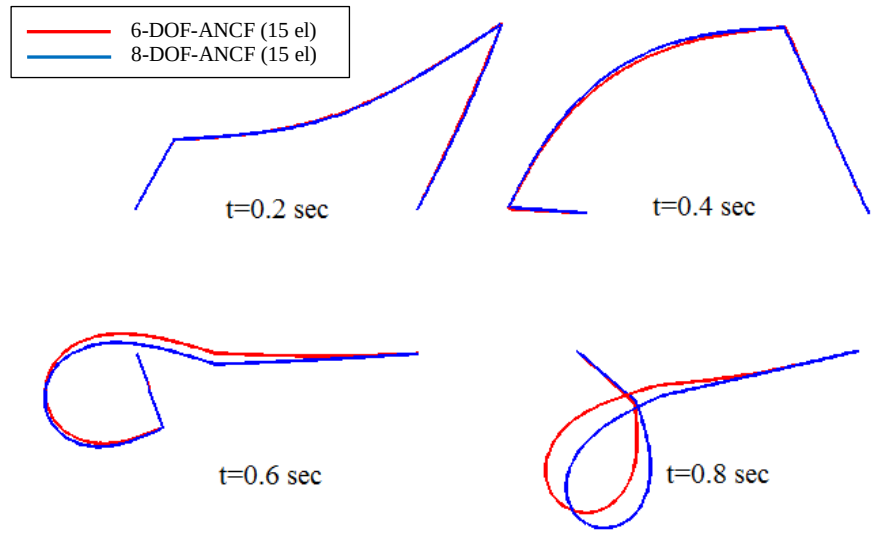

Figure 6.10 Simulation of the four-bar mechanism using 15 elements in the coupler.

As can be seen in Figures 6.6, 6.7 and the simulations, results are in good agreement for all the analyses until 0.65 seconds where deformations are close to the highest level. After that time, results differ especially for the 6-DOF-ANCF beam element type. But results get closer as the element numbers are increased.

In Table 6.5, CPU time ratios are given with respect to the analysis carried out by using the 6-DOF-ANCF beam element type with six elements in the coupler. As can be seen in the table, better computational time can be achieved when 6-DOF-ANCF beam element type is used.

Table 6.5 CPU time ratios of the four-bar mechanism.

	6 Elements	9 Elements	15 Elements
6-DOF-ANCF	1	1.34	1.93
8-DOF-ANCF	2.20	2.32	3.81

CHAPTER 7

RESULTS AND DISCUSSIONS

In this section, the results are presented by using flexible four-bar mechanism simulations and divided into two sub-categories as small-medium and large deformation analyses. All links of the four-bar mechanism are flexible. The crank and the follower are selected with high modulus of elasticity values whereas the coupler is selected to have a different range of modulus of elasticity values so that different orders of deformations are examined.

7.1. Small-Medium Deformation Analyses

In the case of small-medium deformation analyses, the absolute nodal coordinate formulation is used with both the conventional planar ANCF (8-DOF-ANCF) beam element type and the new planar ANCF (6-DOF-ANCF) beam element type. Also the floating frame of reference formulation is used in the analyses to compare the results.

The four-bar mechanism that is used in the analyses is given in Figure 7.1. The crank and the follower are attached to the ground, and the coupler is attached to the links with revolute joints. The mechanism works with the applied moment to the base point of the crank. The gravitational forces also exist in the system.

The results obtained by the developed codes are also compared with the results obtained by ADAMS® software in which the floating frame of reference formulation is used.

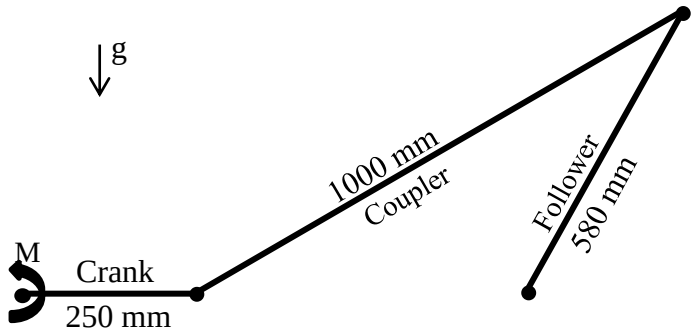

Figure 7.1 Four-bar mechanism for the small-medium deformation analyses.

The moment, $M(t)$, applied to the crank is given in the Equation (7.1). The gravitational acceleration is taken as 9.81 m/s^2.

$$M(t) = \begin{cases} 6\tan^{-1}(20t) & t < 0.5\ sec \\ 0 & t \geq 0.5\ sec \end{cases} \tag{7.1}$$

Depending on the elasticity of the coupler, four different cases are examined which are given in Table 7.1. Other parameters are given in Table 7.2.

Table 7.1 Cases of the small-medium deformation analyses.

	Modulus of Elasticity [GPa]		
	Crank	Coupler	Follower
Case-1	100	0.25	100
Case-2	100	0.20	100
Case-3	100	0.16	100
Case-4	100	0.10	100

Table 7.2 Parameters of the four-bar mechanism for the small-medium deformation analyses.

	Mass [kg]	Cross Sectional Area [mm^2]	Second Moment Of Area [mm^4]
Crank	0.94	$1.3x10^3$	$1.3x10^5$
Coupler	2.94	$2.0x10^3$	$3.1x10^5$
Follower	2.18	$1.3x10^3$	$1.3x10^5$

To generate the flexible links for the analyses made by the floating frame of reference formulation, ANSYS® parametric design language is used. Two-noded beam element (BEAM188) in the library of ANSYS® is selected with the properties and the meshes, and then the links are exported in the form of "MNF file" that is used in the ADAMS® software. Mode numbers and natural frequencies of the beams for different cases are given in Appendix A. Note that first six modes are not used in the analyses since they are rigid body modes Depending on the element numbers in the coupler, different models are generated for all the cases. The model names and the element numbers of the links are given in Table 7.3.

Table 7.3 Model names and used number of finite elements for the small-medium deformation analyses.

	Number of Elements		
	Crank	Coupler	Follower
6-DOF-ANCF (4el)	1	4	2
6-DOF-ANCF (8el)	1	8	2
8-DOF-ANCF (3el)	1	3	2
8-DOF-ANCF (6el)	1	6	2
FFR (25 el)	2	25	5
FFR (50 el)	2	50	5

In all the analyses, Newmark method is used with a γ value of 0.7 and a β value of 0.36. Maximum error and iteration numbers are selected as $1x10^{-3}$ and 75 respectively. Total analysis time is 1 second with time steps of 0.01 seconds.

The distance between the center point of the coupler and the origin of the absolute coordinate system attached to the initial point of the crank is used to represent the results graphically. Figures show the center distance graph and the energy graphs for the coupler, and are separated two categories, corresponding to analyses made by low element numbers and high element numbers.

7.1.1. Case-1

Figures 7.2 and 7.3 show the variation of the center distance of the coupler for low element numbers and high element numbers respectively. Furthermore, the variation of kinetic and strain energies are given in Figures 7.4 and 7.5, respectively.

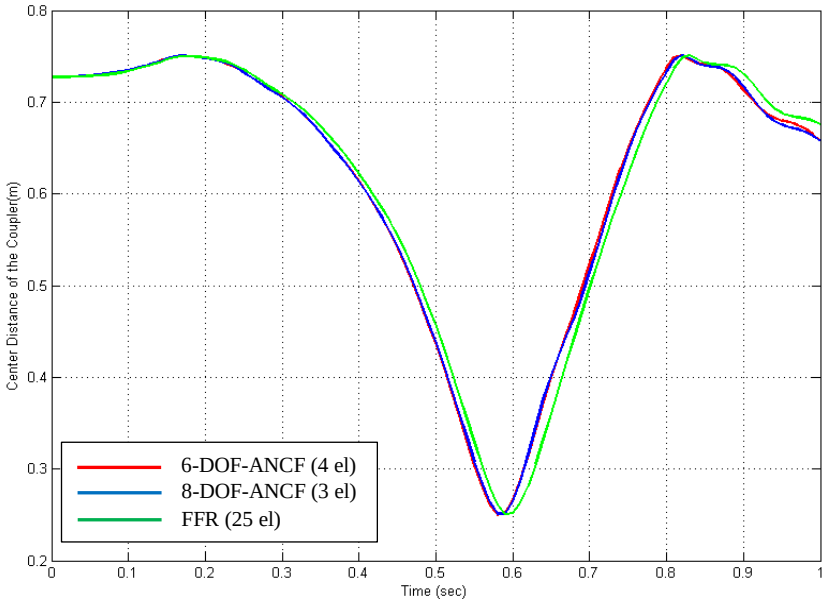

Figure 7.2 Variation of the center distance of the coupler with low element numbers (Case-1)

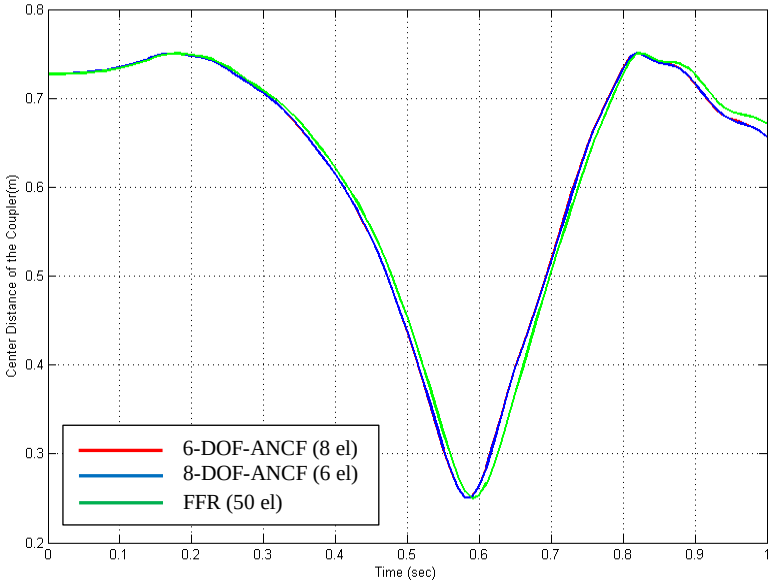

Figure 7.3 Variation of the center distance of the coupler with high element numbers (Case-1)

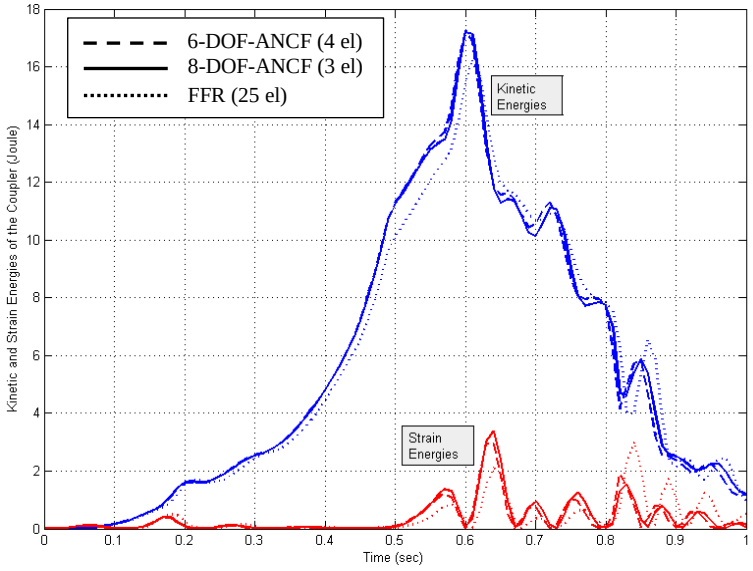

Figure 7.4 Variation of kinetic and strain energies of the coupler with low element numbers (Case-1)

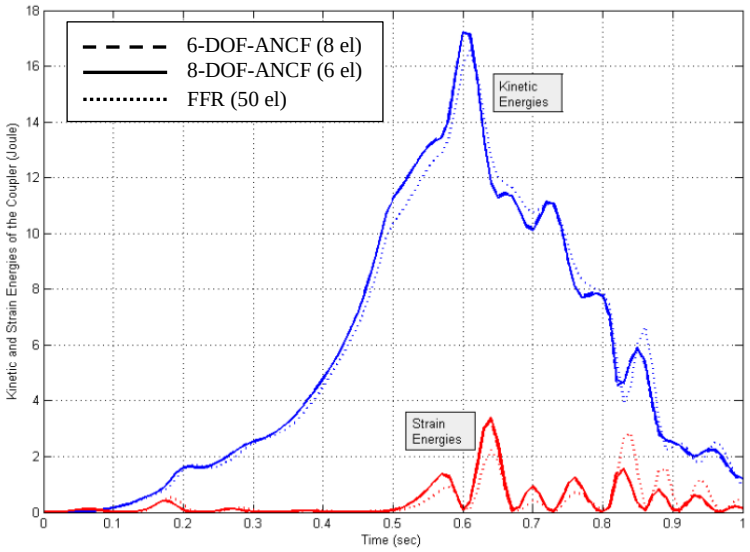

Figure 7.5 Variation of kinetic and strain energies of the coupler with high element numbers (Case-1)

7.1.2. Case-2

The variation of center distance of the coupler is given in Figures 7.6 and 7.7. Also, Figures 7.8 and 7.9 show the variation of kinetic and strain energies of the coupler.

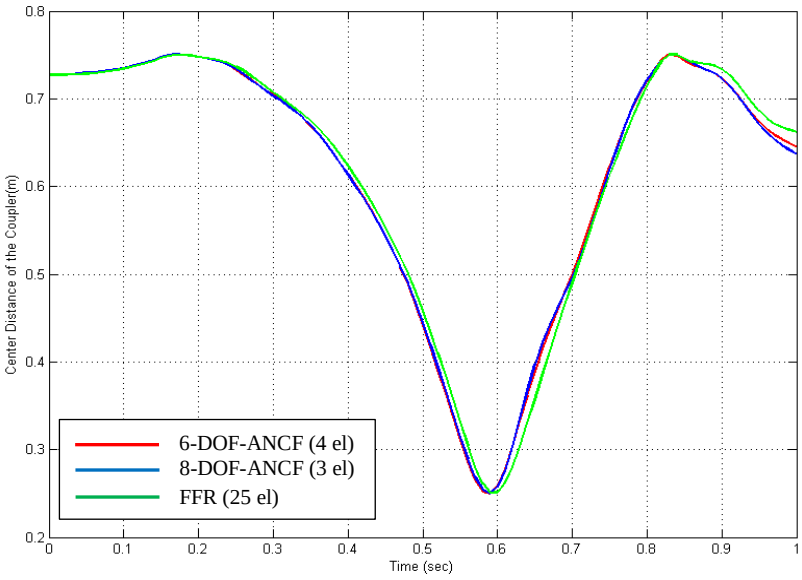

Figure 7.6 Variation of the center distance of the coupler with low element numbers (Case-2)

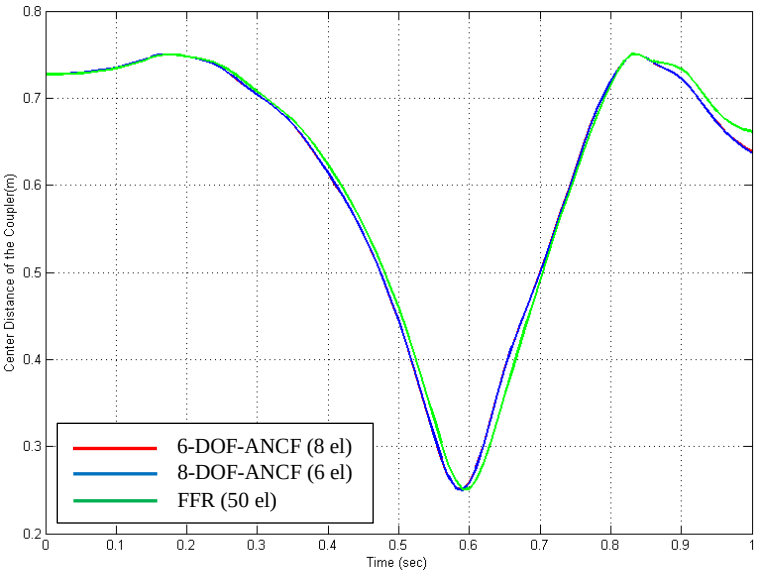

Figure 7.7 Variation of the center distance of the coupler with high element numbers (Case-2)

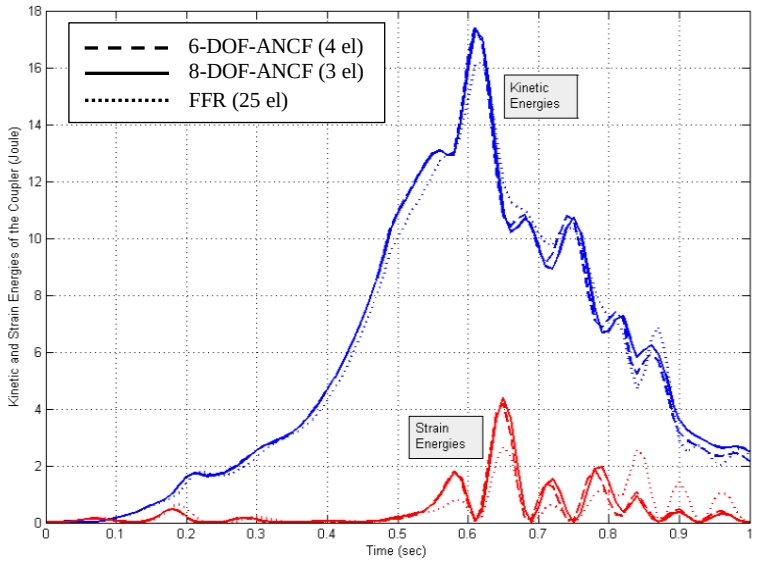

Figure 7.8 Variation of kinetic and strain energies of the coupler with low element numbers (Case-2)

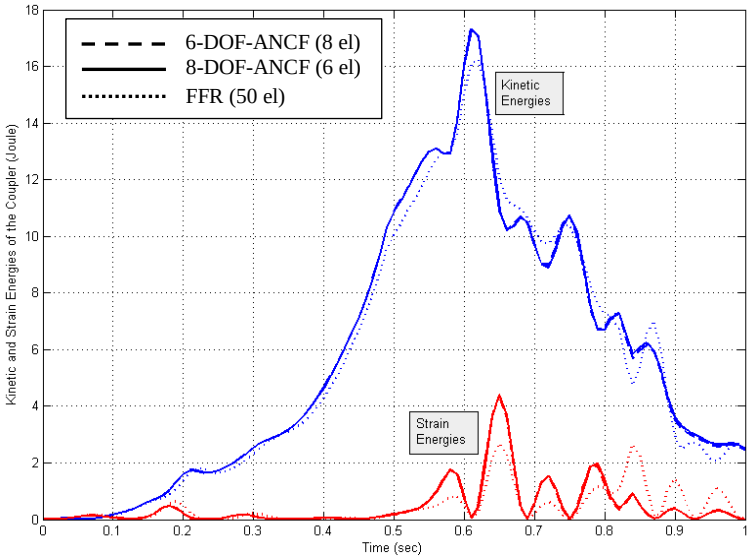

Figure 7.9 Variation of kinetic and strain energies of the coupler with high element numbers (Case-2)

7.1.3. Case-3

Figures 7.10 and 7.11 show the center distance graphs of the coupler. Also, the variation of kinetic and strain energies are given in Figures 7.12 and 7.13.

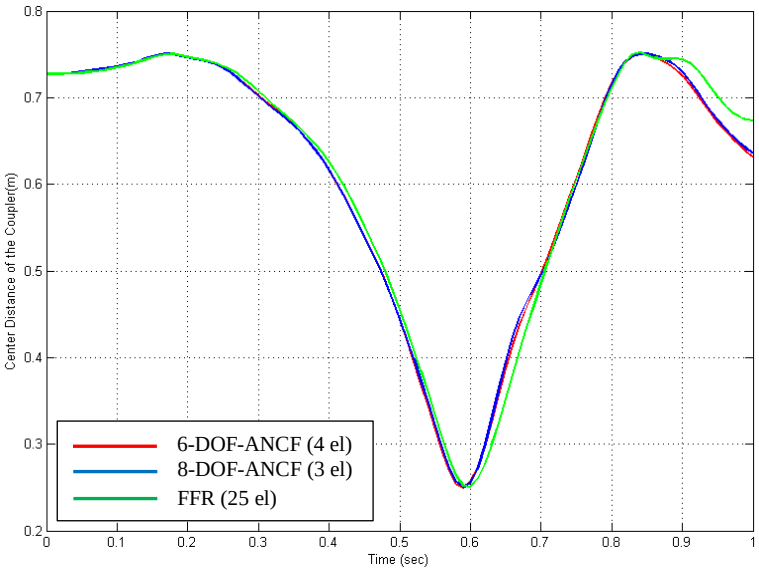

Figure 7.10 Variation of the center distance of the coupler with low element numbers (Case-3)

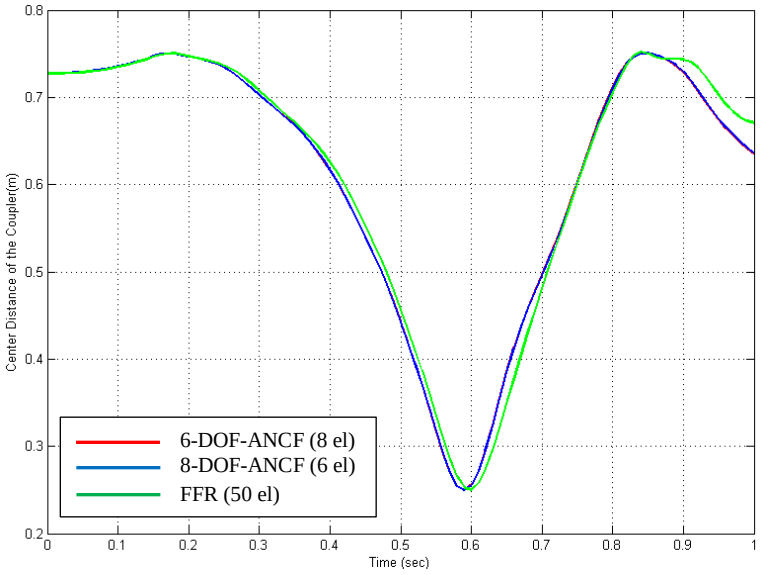

Figure 7.11 Variation of the center distance of the coupler with high element numbers (Case-3)

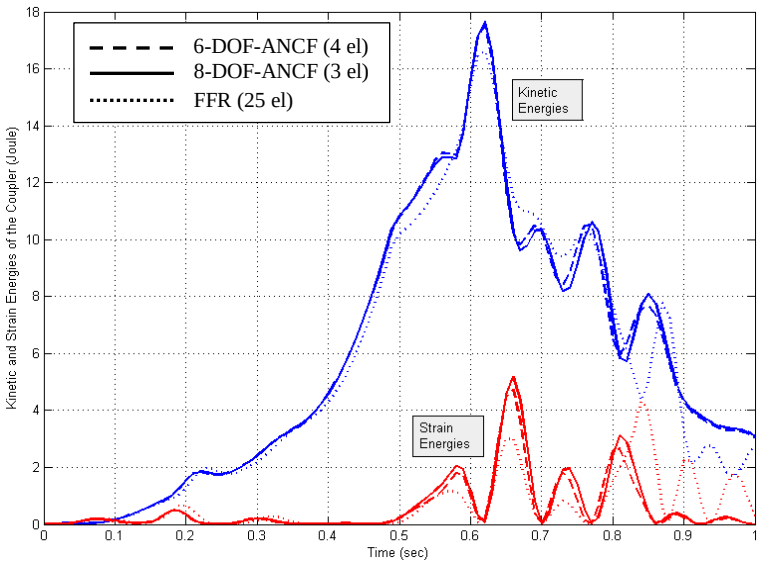

Figure 7.12 Variation of kinetic and strain energies of the coupler with low element numbers (Case-3)

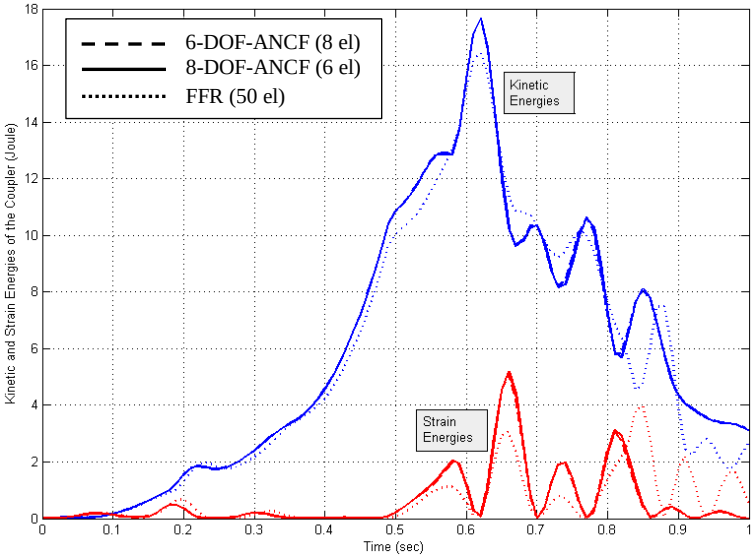

Figure 7.13 Variation of kinetic and strain energies of the coupler with high element numbers (Case-3)

7.1.4. Case-4

Figures 7.14 and 7.15 show the variation of center distance of the coupler. The variation of kinetic and strain energies are also given in Figures 7.16 and 7.17.

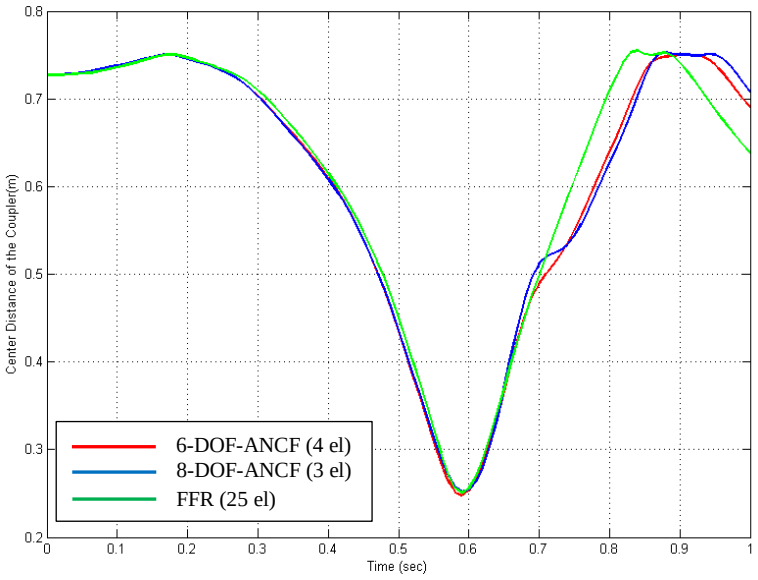

Figure 7.14 Variation of the center distance of the coupler with low element numbers (Case-4)

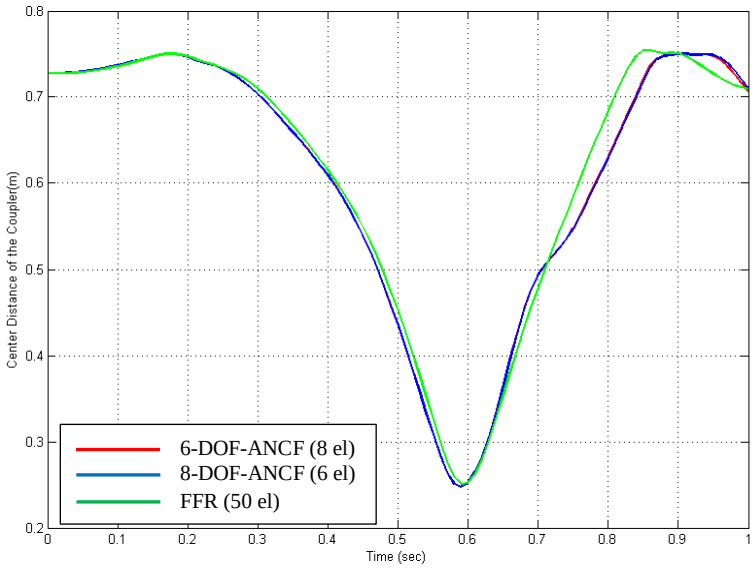

Figure 7.15 Variation of the center distance of the coupler with high element numbers (Case-4)

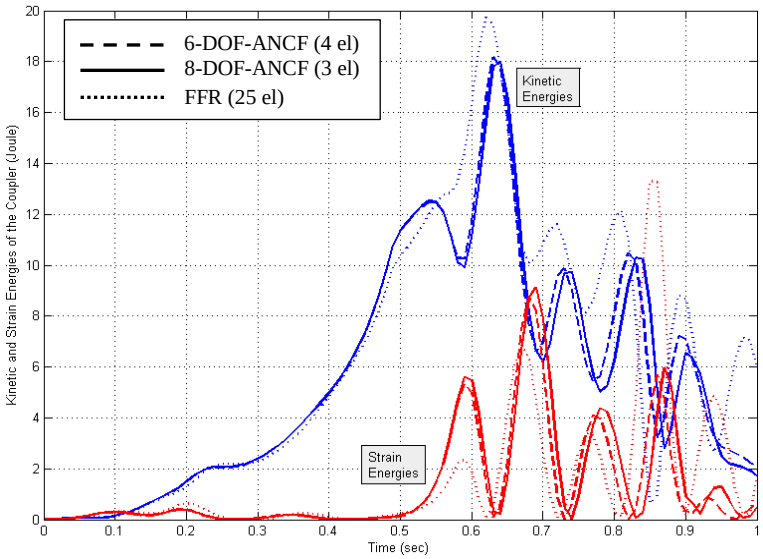

Figure 7.16 Variation of kinetic and strain energies of the coupler with low element numbers (Case-4)

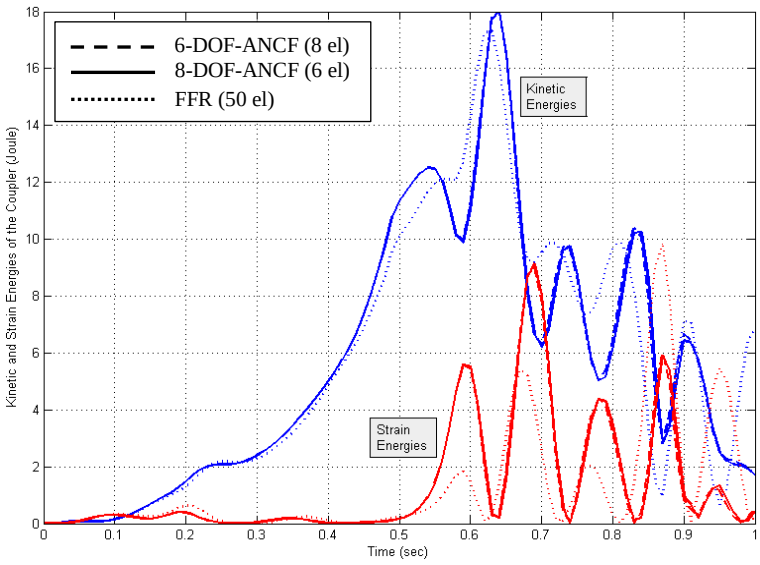

Figure 7.17 Variation of kinetic and strain energies of the coupler with high element numbers (Case-4)

7.1.5. Discussions about the Small-Medium Deformation Analyses Results

The modulus of elasticity values are selected to decrease from Case-1 to Case-4 in order to see the capability of the methods for handling the small to medium deformations. Since the crank and the follower are taken to be rigid enough, only the results of the coupler are presented.

In all the analyses, deformations become larger at the second half of the analysis time since the moment is not used anymore to overcome the gravitational forces. In the second half of the analysis time, both the bending moment and the gravitational forces accelerate the system so that deformations increase in the coupler. When deformations get higher in magnitude, it is seen that the kinetic energy decreases with increasing the strain energy. The kinetic energy of the coupler oscillates at the second half of the analysis time. Oscillations are larger when the coupler is more elastic as expected.

For all the cases, the results of the analyses using both the 6-DOF-ANCF beam element type and the 8-DOF-ANCF beam element type are in very good agreement,

and they don’t change considerably when high element numbers are used. It shows that in the case of small-medium deformations, even small number of elements can handle the analyses if the absolute nodal coordinate formulation is used with both element types.

Results of first two cases are in good agreement for both the absolute nodal coordinate formulation and the floating frame of reference formulation. At the second half of the analyses, where deformations get larger, results obtained by the floating frame of reference formulation are seen slightly different from the absolute nodal coordinate formulation in the third case. Differences in the results increase considerably in the Case-4 where deformations are no longer small. It shows that the floating frame of reference formulation is not appropriate for large deformation problems.

7.2. Large Deformation Analyses

Since the floating frame of reference formulation is not capable of solving large deformation problems, only results of the absolute nodal coordinate formulation are presented here. The four-bar mechanism that is used in the large deformation analyses is given in Figure 7.18.

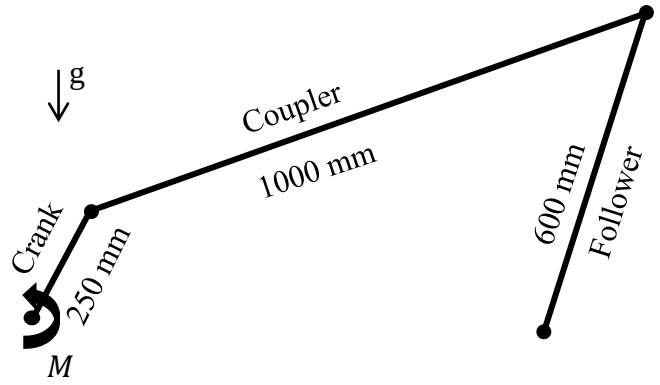

Figure 7.18 Four-bar mechanism for the large deformation analyses.

Gravitational forces exist, and the system works with the moment applied to the crank. Model names and the number of elements used in the links are given in Table 7.4. Depending on the elasticity of the coupler, three cases are examined as given in Table 7.5 with different element numbers in the coupler.

Table 7.4 Model names and used number of finite elements for the large deformation analyses.

	Number of Elements		
	Crank	Coupler	Follower
6-DOF-ANCF (5)	1	5	2
6-DOF-ANCF (10)	1	10	2
6-DOF-ANCF (15)	1	15	2
8-DOF-ANCF (5)	1	5	2
8-DOF-ANCF (10)	1	10	2
8-DOF-ANCF (15)	1	15	2

Table 7.5 Cases of large deformation analyses.

	Modulus of Elasticity [GPa]		
	Crank	Coupler	Follower
Case-5	200	1.2×10^{-2}	200
Case-6	200	8.0×10^{-3}	200
Case-7	200	5.0×10^{-3}	200

The Newmark method is used with a γ value of 0.75 and a β value of 0.39. Maximum error and iteration numbers are selected as 1×10^{-3} and 75 respectively.

Total analysis time is 0.9 seconds with time steps of 0.01 seconds. The moment, $M(t)$, applied to the crank is given in Equation (7.2). The gravitational acceleration is taken as 9.81 m/s^2.

$$M(t) = \begin{cases} 6 \sin \dfrac{\pi t}{0.6} & t < 0.6\ sec \\ 0 & t \geq\ 0.6\ sec \end{cases} \tag{7.2}$$

Other parameters that are used in the analyses are given in Table 7.6.

Table 7.6 Parameters of four-bar mechanism for the large deformation analyses.

	Mass [kg]	Cross Sectional Area [mm^2]	Second Moment Of Area [mm^4]
Crank	0.53	2.1x10^3	6.0x10^5
Coupler	2.95	2.0x10^3	3.1x10^5
Follower	1.57	1.6x10^3	5.1x10^5

The mid-point transverse deflection, the kinetic energy and the strain energy graphs of the coupler are presented here as the results. Also, simulation results are given for the 0.3 sec, 0.6 sec and 0.9 sec. of the analysis time.

7.2.1. Case-5

Figure 7.19 shows the transverse mid-point deflection of the coupler. Kinetic energy and strain energy graphs of the coupler are given in Figures 7.20 and 7.21 respectively. Also, simulation results are given in Figure 7.22.

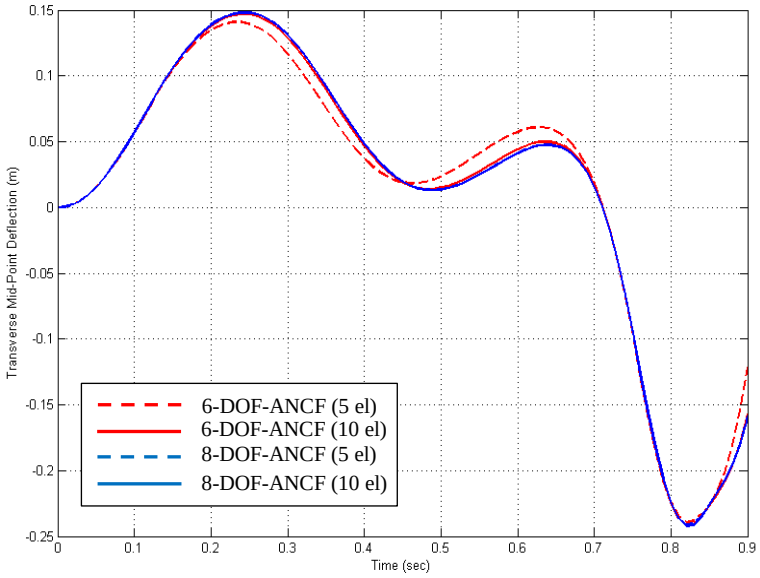

Figure 7.19 Variation of the transverse mid-point deflection of the coupler (Case-5).

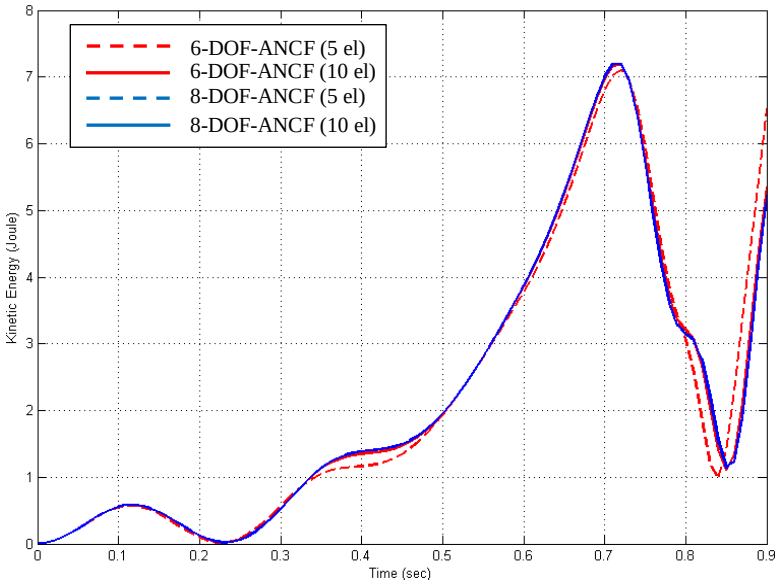

Figure 7.20 Variation of the kinetic energy of the coupler (Case-5).

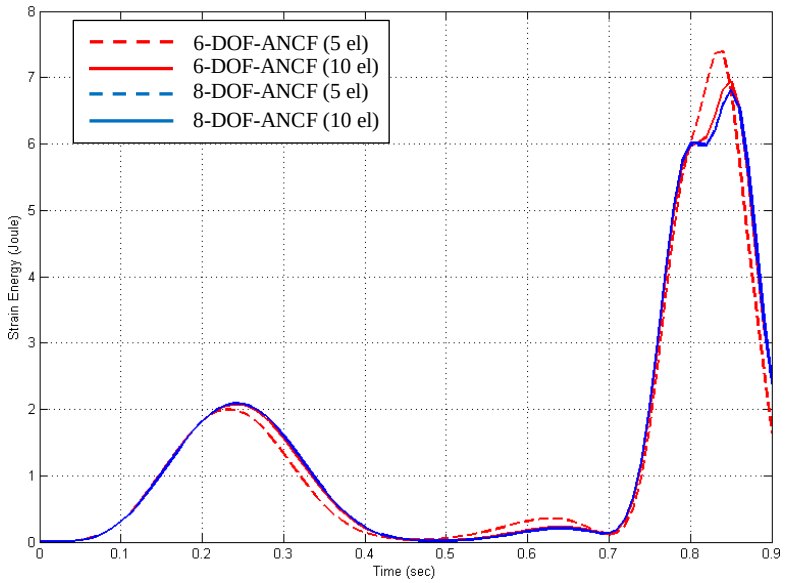

Figure 7.21 Variation of the strain energy of the coupler (Case-5).

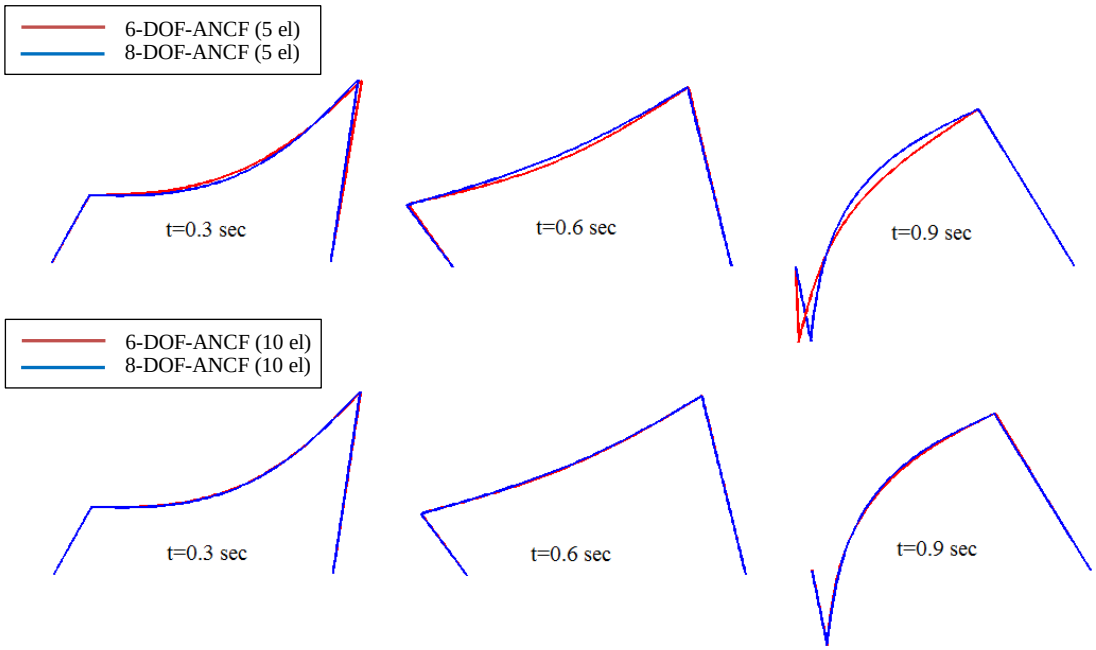

Figure 7.22 Simulation results (Case-5).

7.2.2. Case-6

The transverse mid-point deflection graph is given in Figure 7.23 for the coupler. Also, kinetic and strain energy graphs are given in Figures 7.24 and 7.25 respectively. At the end, simulation results are shown in Figure 7.26.

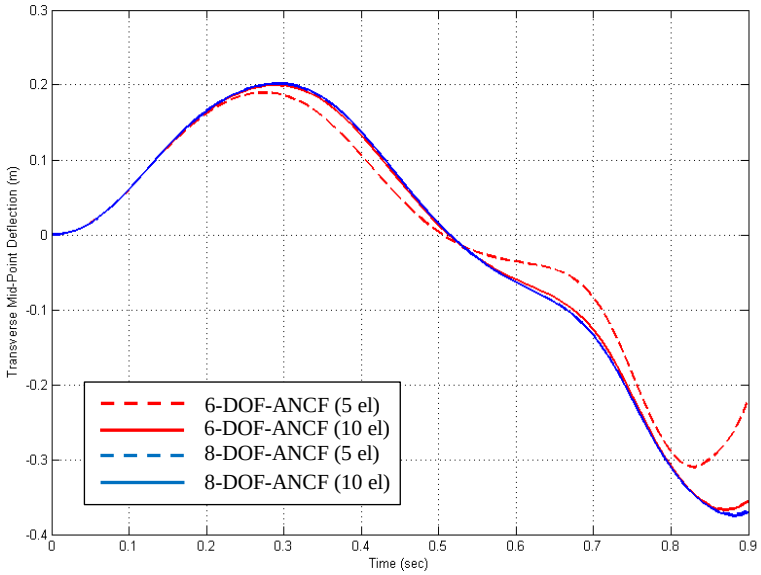

Figure 7.23 Variation of the transverse mid-point deflection of the coupler (Case-6).

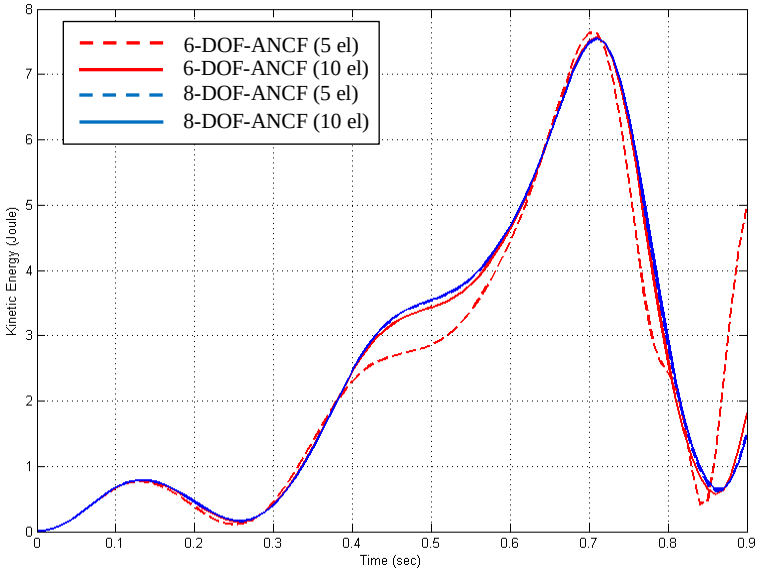

Figure 7.24 Variation of the kinetic energy of the coupler (Case-6).

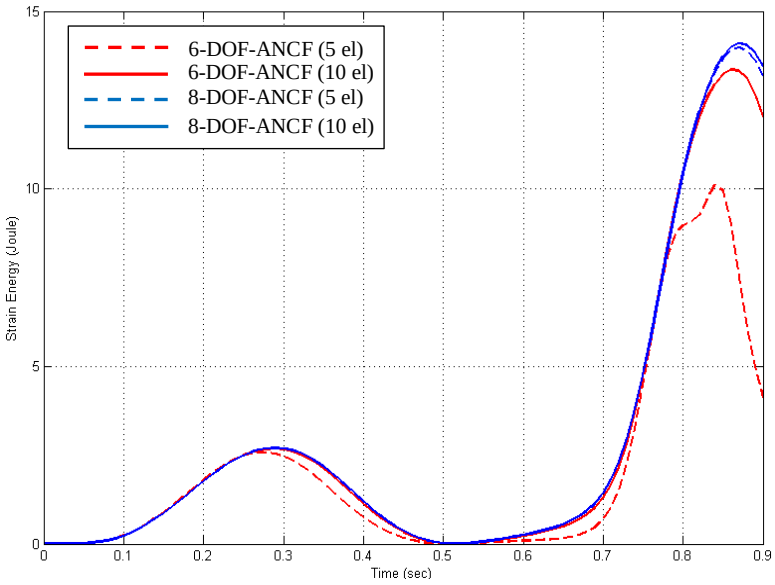

Figure 7.25 Variation of the strain energy of the coupler (Case-6).

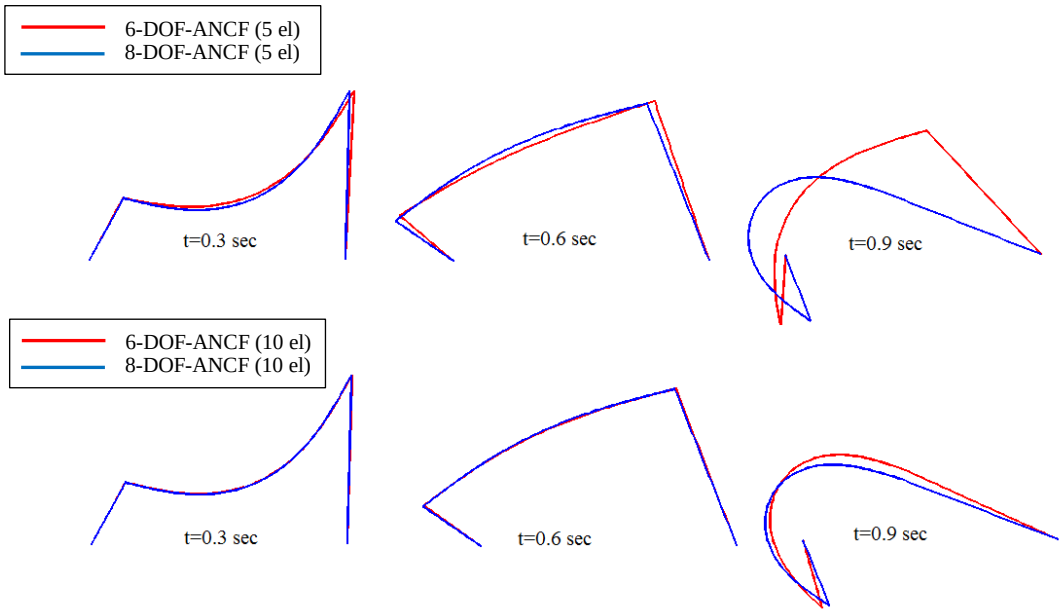

Figure 7.26 Simulation results (Case-6).

7.2.3. Case-7

The transverse mid-point deflection of the coupler is given in Figure 7.27. Kinetic energy and strain energy graphs of the coupler are shown in Figures 7.28 and 7.29 respectively. Also, simulation results are shown in Figure 7.30.

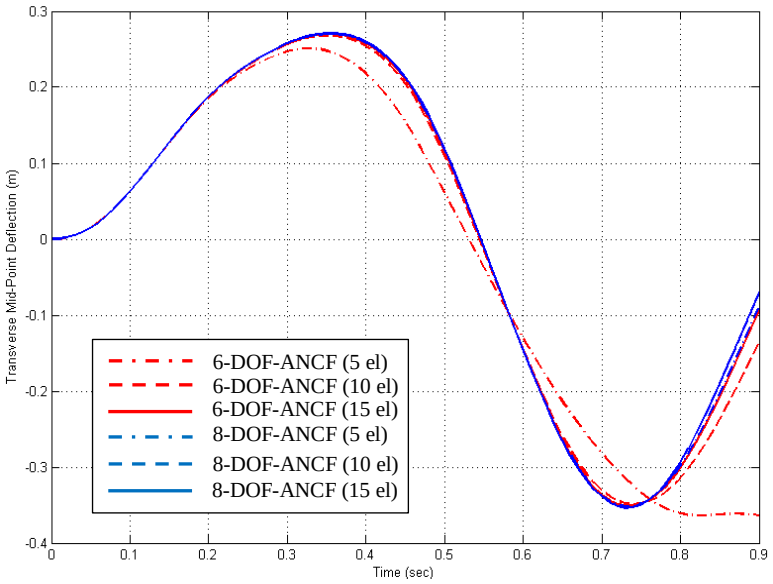

Figure 7.27 Variation of the transverse mid-point deflection of the coupler (Case-7).

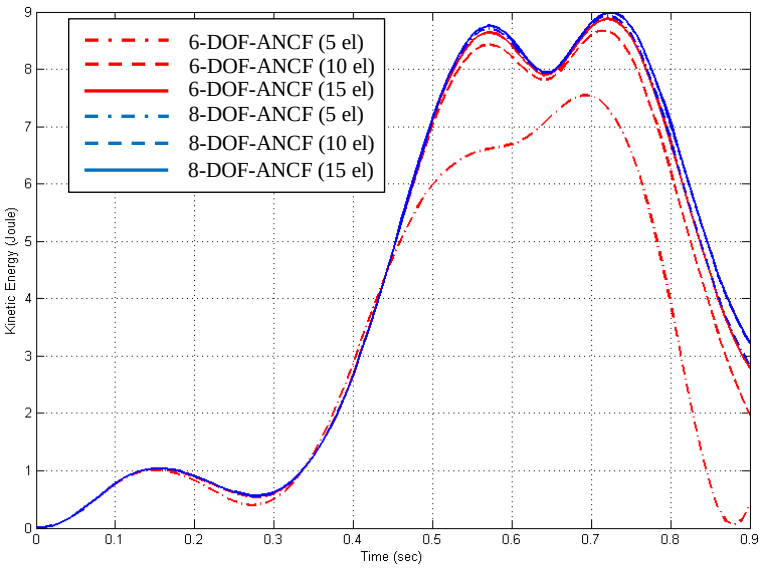

Figure 7.28 Variation of the kinetic energy of the coupler (Case-7).

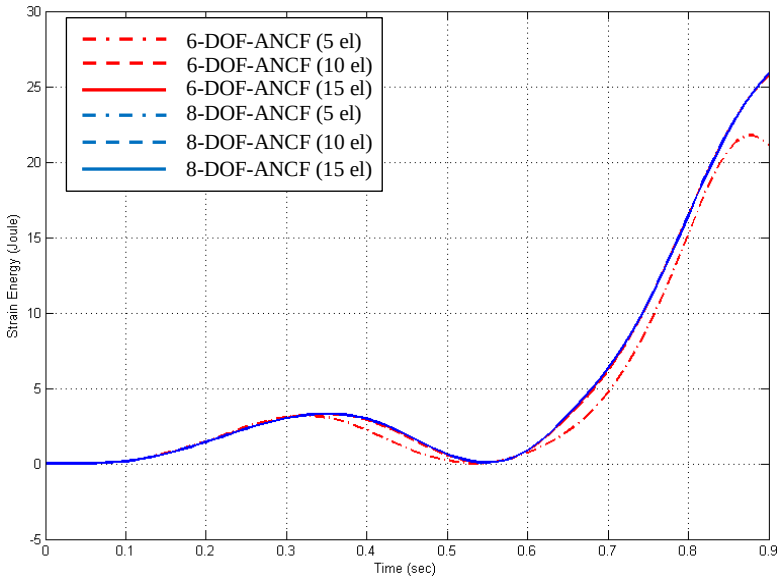

Figure 7.29 Variation of the strain energy of the coupler (Case-7).

Figure 7.30 Simulation results (Case-7).

7.2.4. Discussions about the Large Deformation Analyses Results

Rigidity of the coupler is reduced from Case-5 to Case-7 in order to see the deformation changes and the capability of the element types for handling the analyses. In all cases, results of the analyses made by the 8-DOF-ANCF beam element type are similar to each other when low and high element numbers are used. It shows that accuracy of that element type is good even when low element numbers are used in the links. In the fifth case, the 6-DOF-ANCF beam element type gives relevant results as compared to the 8-DOF-ANCF beam element type. In the sixth case, results are not same for the couplers with low element numbers toward the end of the analyses where deformations are large, but results become similar when element numbers are increased. In the seventh case, deformations become larger especially toward the end of the analyses. To handle the deformations in the Case-7, more elements are needed in the coupler for the 6-DOF-ANCF beam element type as compared to other cases.

In the small deformation analyses, the strain energies are lower as compared to the kinetic energies. Also, there is a correlation between them so that when kinetic energy is decreased, strain energy is increased. As shown in the figures, strain energies are very high in the large deformation analyses, and there are no obvious correlations in the energies.

CHAPTER 8

CONCLUSIONS AND FUTURE WORK

8.1. Conclusions

In this thesis, the absolute nodal coordinate formulation is used for the analyses of planar flexible multibody systems. For this purpose, two different planar beam types are considered. First type is the conventional ANCF planar (8-DOF-ANCF) beam element, and the other is the developed ANCF planar (6-DOF-ANCF) beam element. In the 6-DOF-ANCF beam element, neither slopes nor angles are used to define the orientation of the beam whereas global slopes are used in the conventional type in addition to positions. In the absolute nodal coordinate formulation, elastic forces are derived from the shape functions, and composed of the element nodal coordinates. First of all, the 6-DOF-ANCF beam element type has quadratic shape function polynomials instead of cubic ones. Also, the element has six degrees of freedom, which is lower than that of the 8-DOF-ANCF beam element. Therefore, the following conclusions are acquired in the study:

1. The proposed element requires a constraint equation for the connection of two consecutive elements to satisfy the continuity of the slopes. In the developed algorithm, an additional constraint equation is added automatically which causes increase in the number of algebraic equations in the equations of motion.
2. Differential algebraic equations (DAEs) are solved with the direct integration method in this study. This procedure is fast and easy to apply, but stability can be affected as the algebraic equation number is increased when a large number of elements are used.

3. In the small to medium deformation cases, accuracies of the 6-DOF-ANCF beam element type are similar to the 8-DOF-ANCF beam element type.
4. In the small deformation cases, accuracies of the floating frame of reference formulation (FFR) are seen to be relevant to the ANCF beam element types. Since FFR is not suitable for large deformation analyses, it is not compared with ANCF in the large deformation cases.
5. In the large deformation cases, the 8-DOF-ANCF beam element type is more accurate than the 6-DOF-ANCF beam element type. Although results converge as the element numbers are increased, high element numbers can be required for the 6-DOF-ANCF beam element type to get accurate results when deformations are very large.
6. The elastic force equations are simpler in the proposed element type. Moreover, the mass matrix and the external force equations become simpler.
7. The analyses in the study show that the structure of the 6-DOF-ANCF beam element type decreases the computational time considerably. Hence the 6-DOF-ANCF beam element may be a good alternative for both the small and large deformation cases.

7.2. Future Work

In the study, numerical damping that is introduced by the Newmark method leads to some numerical errors in the analyses. As a future work, Hilber-Hughes-Taylor or other methods that do not introduce numerical damping may be used to diminish such numerical errors. Also, Wehage's partitioning technique can be used to see the stability when high numbers of 6-DOF-ANCF beam elements are used in the case of large deformations. Since only the independent variables are integrated, this method is believed to give better results.

In the future, shear deformations can be considered, since shear deformations are neglected in the developed beam element. Also, the logic of the Bezier surfaces can be applied to solve flexible multibody systems involving plate elements in ANCF. However, connections of the elements might be more difficult than the planar beam elements.

REFERENCES

[1] Shabana, A.A., "Flexible Multibody Dynamics: Review of Past and Recent Developments", *Multibody System Dynamics*, **1**: 189-222, 1997.

[2] Shabana, A.A., *Computational Dynamics,* Wiley, New York, 2001.

[3] Shabana, A.A., *Dynamics of Multibody Systems,* Cambridge University Press, Cambridge, 2005.

[4] Seo J., Kim S., Jung S., Park T., Mok J., Kim Y. and Chai J., "Dynamic Analysis of a Pantograph-Catenary System Using Absolute Nodal Coordinates", *Vehicle System Dynamics*, Vol.44, No.8, 615-630, 2006.

[5] Berzeri M., Campanelli M., and Shabana A., "Definition of the Elastic Forces in the Absolute Nodal Coordinate Formulation and the Floating Frame of Reference Formulation", *Multibody System Dynamics*, **5**, 21-54, 2001.

[6] Shabana, A.A., *Computational Continuum Mechanics,* Cambridge University Press, Cambridge, 2008.

[7] Berzeri M. and Shabana,A.A., "Development of Simple Models for the Elastic Forces in the Absolute Nodal Co-ordinate Formulation", *Journal of Sound and Vibration*, **235**(4), 539-565, 2000.

[8] Shabana A.A. "Definition of the Slopes and the Finite Element Absolute Nodal Coordinate Formulation", *Multibody System Dynamics*, **1**: 339-348, 1997.

[9] Berzeri M.., "Definition of the Elastic Forces in the Finite Element Formulations", *Technical Report No. MBS98-1-UIC*, University of Illinois at Chicago, 1998.

[10] Yoo W.S., Lee S.P., Sohn J., Dmitrochenko O. and Pogorelov D. "Large Oscillations of a Thin Cantilever Beam: Physical Experiments and Simulation Using the Absolute Nodal Coordinate Formulation", *Nonlinear Dynamics*, **34**: 3-29, 2003.

[11] Omar A.O. and Shabana A.A., "Development of a Shear Deformable Element Using the Absolute Nodal Coordinate Formulation", *Technical Report No. MBS00-3-UIC*, University of Illinois at Chicago, 2000.

[12] Reddy, J.N., *An Introduction to the Finite Element Method*, McGraw-Hill, New York, 2006.

[13] Escalona J.L., Hussien H.A. and Shabana A.A., "Application of the Absolute Nodal Coordinate Formulation to Multibody System Dynamics", *Journal of Sound and Vibration*, **214**(5), 833-851, 1998.

[14] Timoshenko S., *Strength of Materials*, 3rd edition, Krieger Publishing Company, New York, 1976.

[15] Greenberg, M.D., *Advanced Engineering Mathematics*, 2nd edition, Prentice-Hall, Englewood Cliffs, NJ, 1998.

[16] Goetz A., *Introduction to Differential Geometry*, Addison Wesley Publishing Company, London, 1970.

[17] Lin S. and Huang J., "Numerical Integration of Multibody Mechanical Systems Using Baumgarte`s Constraint Stabilization Method.", *Journal of the Chinese Institute of Engineers*, Vol.25, No:2, pp. 243-252, 2002.

[18] Wehage R.A. and Haug E.J., "Generalized Coordinate Partitioning for Dimension Reduction in Analysis of Constrained Dynamic Systems", *Journal of Mechanical Design,* Vol. 104/**247**, 1982.

[19] Baumgarte J., 1972, "Stabilization of Constraints and Integrals of Motion in Dynamic Systems", *Computer Methods in Applied Mechanics and Engineering,* Vol.1, pp. 1-16, 1972.

[20] Shabana A.A., Bauchau O.A. and Hulbert G.M., "Integration of Large Deformation Finite Element and Multibody System Algorithms.", *Journal of Computational and Nonlinear Dynamics,* Vol.2 /**351**, 2007.

[21] Hussein B., Negrut D. and Shabana A.A., "Implicit and Explicit Integration in the Solution of the Absolute Nodal Coordinate Differential/Algebraic Equations", *Nonlinear Dynamics,* 54:283-296, 2008.

[22] Newmark N.M., "A Method of Computation for Structural Dynamics.", *J. Engrg. Mech. Div*., **112**, pp. 67-94, 1959.

[23] Gavrea B., Negrut D. and Potra F.A., "The Newmark Integration Method for Simluation of Multibody Systems: Considerations.", *ASME International Mechanical Engineering Congress and Exposition IMECE 2005-81770,* 2005.

[24] Hilber H.M., Hughes T.J.R. and Taylor R.L., "Improved Numerical Dissipation for Time Integration Algorithms in Structural Dynamics", *Earthquake Eng. And Struct. Dynamics*, **5**, pp. 283-292, 1977.

[25] Korovkin P.P, "Bernstein Polynomials" In Hazewinkel, Michiel, Encyclopedia of Mathematics, Springer, ISBN 979-1-55608-010-4, 2001.

APPENDIX A

The Mode Numbers and the Natural Frequencies

Table A.1 The mode numbers and the natural frequencies of the coupler for Case-1.

Mode Numbers	Natural Frequencies [Hz]	
	Case-1 25 Elements	Case-1 50 Elements
7	17.91	17.96
8	17.91	17.96
9	48.58	48.78
10	48.59	48.79
11	93.36	93.80
12	93.36	93.80
13	144.86	144.95
14	150.67	151.38
15	150.79	151.54
16	204.86	204.99
17	219.17	220.21
18	219.17	220.21
19	290.33	291.03
20	297.02	298.36
21	297.16	298.81
22	382.95	384.98
23	382.95	384.98
24	466.07	468.26
25	475.42	477.86
26	499.12	504.33
27	664.35	676.53
28	705.86	713.23
29	832.16	923.76
30	990.70	1108.86
31	990.70	1108.86
32	1150.06	1295.01

Table A.2 The mode numbers and the natural frequencies of the coupler for Case-2.

Mode Numbers	Natural Frequencies [Hz]	
	Case-2 25 Elements	Case-2 50 Elements
7	16.02	16.07
8	16.02	16.07
9	43.45	43.63
10	43.46	43.64
11	83.50	83.90
12	83.50	83.90
13	129.57	129.65
14	134.77	135.40
15	134.87	135.54
16	183.24	183.35
17	196.03	196.96
18	196.03	196.96
19	259.68	260.30
20	265.67	266.86
21	265.79	267.26
22	342.52	344.34
23	342.52	344.34
24	416.87	418.82
25	425.22	427.41
26	446.43	451.08
27	594.21	605.11
28	631.34	637.93
29	744.30	826.24
30	886.11	991.79
31	886.11	991.79
32	1028.65	1158.29

Table A.3 The mode numbers and the natural frequencies of the coupler for Case-3.

Mode Numbers	Natural Frequencies [Hz]	
	Case-3 25 Elements	Case-3 50 Elements
7	14.33	14.37
8	14.33	14.37
9	38.86	39.03
10	38.87	39.04
11	74.69	75.04
12	74.69	75.04
13	115.89	115.96
14	120.54	121.10
15	120.63	121.23
16	163.89	163.99
17	175.33	176.17
18	175.33	176.17
19	232.26	232.82
20	237.62	238.68
21	237.73	239.05
22	306.36	307.98
23	306.36	307.98
24	372.86	374.61
25	380.33	382.28
26	399.30	403.46
27	531.48	541.23
28	564.69	570.58
29	665.72	739.01
30	792.56	887.09
31	792.56	887.09
32	920.05	1036.01

Table A.4 The mode numbers and the natural frequencies of the coupler for Case-4.

Mode Numbers	Natural Frequencies [Hz]	
	Case-4 25 Elements	Case-4 50 Elements
7	11.33	11.36
8	11.33	11.36
9	30.72	30.85
10	30.73	30.86
11	59.05	59.32
12	59.05	59.32
13	91.62	91.68
14	95.29	95.74
15	95.37	95.84
16	129.57	129.65
17	138.61	139.28
18	138.61	139.28
19	183.62	184.06
20	187.85	188.70
21	187.94	188.98
22	242.20	243.48
23	242.20	243.48
24	294.77	296.15
25	300.68	302.22
26	315.67	318.96
27	420.17	427.88
28	446.43	451.08
29	526.30	584.24
30	626.57	701.30
31	626.57	701.30
32	727.36	819.04

Table A.5 The mode numbers and the natural frequencies of the crank and the follower.

Mode Numbers	**Natural Frequencies [Hz]**	
	Crank	**Follower**
7	2144.79	550.10
8	2144.79	550.10
9	7351.05	1460.52
10	10395.96	1460.52
11	10395.96	2920.37
12	10395.96	2920.37
13	10395.96	3481.14
14	14702.10	5270.44
15	24483.66	5270.44
16	24483.66	5305.16
17	31991.86	6614.91
18	31991.86	9367.87
19	-	9992.85
20	-	10703.15
21	-	13531.96
22	-	13531.96
23	-	17807.08
24	-	17807.08